

36430120

**STUDY OF DEFORMATION
PROCESSING OF
STRUCTURAL POROUS METALS**

A Thesis Presented to
The Faculty of the
Fritz J. and Dolores H. Russ
College of Engineering and Technology
Ohio University

In Partial Fulfillment
of the Requirement for the Degree of

Master of Science

by

Shatil S. Ahmed

November, 1996

Thesis
M
1996
AHME

ms 131 010109

ACKNOWLEDGEMENT

I begin my acknowledgement by thanking the all mighty Allah foremost for providing me with the knowledge and opportunity to complete this thesis.

I wish to acknowledge my thanks and gratitude to my thesis advisor, Dr. M.K. Alam for his continuous guidance, support and patience. I am grateful Dr. J. Gunasekera for his valuable time and advice. I owe my thanks to Dr. H. Pasic for his excellent teaching in the field of continuum mechanics and plasticity, which helped me all throughout. I express my special appreciation to the faculty, staff, and fellow students in the Department of Mechanical Engineering, for their help and cooperation.

I am thankful to Dr. H.L. Gegel and Dr. G.C. Huang of UES Inc., for their extensive support in making the research successful and providing the opportunity to use their facility during the research.

I am deeply grateful to my wife, Kaniz and my parents for their encouragement and support.

3.2.3 Derivation of Stress-Strain Relation for SPM.....	28
4 Testing and Modification of Antares for SPM	33
4.1 Analysis of P/M materials.....	33
4.2 Multi-Group of elements	34
4.3 Multi-Stage Problem.....	35
5 Experiments on SPM.....	37
5.1 Blister Formation in SPM Can Rolling.....	37
5.1.1 Effect of Strain-Rate.....	38
5.1.2 Effect of Differential Thermal Expansion Coefficient and Interfacial Defect.	42
5.1.3 Improper Sintering or Bonding of the P/M Material.....	42
5.2 Compression Test of LDC of SPM.....	43
6 Conclusion and Future Work.....	44
References.....	46
A Results and Analysis of Compression test of LDC of SPM	48
B Code for reading multi-group 2D elements from IDEAS to ANTARES	66

List of Tables

Table A1: Stress-Strain data for 100% dense Ti-6Al-4V at strain rate 0.001sec^{-1}	54
Table A2: Stress-Strain data for 65% dense Ti-6Al-4V SPM at strain rate 0.001sec^{-1}	54
Table A3: Stress-Strain data for 100% dense Ti-6Al-4V at strain rate 0.01sec^{-1}	56
Table A4: Stress-Strain data for 65% dense Ti-6Al-4V SPM at strain rate 0.01sec^{-1}	56
Table A5: Stress-Strain data for 100% dense Ti-6Al-4V at strain rate 0.1sec^{-1}	58
Table A6: Stress-Strain data for 65% dense Ti-6Al-4V SPM at strain rate 0.1sec^{-1}	58
Table A7: Stress-Strain data for 100% dense Ti-6Al-4V at strain rate 1.0sec^{-1}	60

Table A8: Stress-Strain data for 65% dense Ti-6Al-4V SPM at strain rate 1.0sec^{-1}	60
Table A9: Stress-Strain data for 100% dense Ti-6Al-4V at strain rate 10.0sec^{-1}	62
Table A10: Stress-Strain data for 65% dense Ti-6Al-4V SPM at strain rate 10.0sec^{-1}	62
Table A11: Dimension and Density of LDC of SPM before compression test	64
Table A12: Density measurement data of LDC of SPM post compression test.....	65

List of Figures

Figure 2.1: Plot of Tresca's Criterion in a biaxial state.....	8
Figure 2.2: Plot of von Mises Criterion in a biaxial state.....	9
Figure 3.1: Decomposition of incremental stress vector.....	23
Figure 5.1: Effective strain rate contour of first pass of SPM rolling.....	39
Figure 5.2: Effective strain rate contour second pass of SPM rolling	40
Figure 5.3: Effective strain rate contour of rolling with dense face sheet and LDC of Ti-6Al-4V	41
Figure A1: Comparison of Stress-Strain curves of I/M, P/M, and SPM of Ti-6Al-4V at 0.001 strain rate and temperature 1382°F and 1472°F.....	52
Figure A2: Comparison of Stress-Strain curves of I/M, P/M, and SPM of Ti-6Al-4V at 0.001 strain rate and temperature 1562°F, 1652°F, and 1742 °F	53
Figure A3: Stress-Strain curves for 100% dense I/M and 65% dense SPM of Ti-6Al-4V at 0.001 strain rate and temperature 1382°F and 1472°F	55
Figure A4: Stress-Strain curves for 100% dense I/M and 65% dense SPM of Ti-6Al-4V at 0.001 strain rate and temperature 1562°F, 1652°F, and 1742 °F	55
Figure A5: Stress-Strain curves for 100% dense I/M and 65% dense SPM	

	of Ti-6Al-4V at 0.01 strain rate and temperature 1382°F and 1472°F	57
Figure A6:	Stress-Strain curves for 100% dense I/M and 65% dense SPM of Ti-6Al-4V at 0.01 strain rate and temperature 1562°F, 1652°F, and 1742 °F	57
Figure A7:	Stress-Strain curves for 100% dense I/M and 65% dense SPM of Ti-6Al-4V at 0.1 strain rate and temperature 1382°F and 1472°F	59
Figure A8:	Stress-Strain curves for 100% dense I/M and 65% dense SPM of Ti-6Al-4V at 0.1 strain rate and temperature 1562°F, 1652°F, and 1742 °F	59
Figure A9:	Stress-Strain curves for 100% dense I/M and 65% dense SPM of Ti-6Al-4V at 1.0 strain rate and temperature 1382°F and 1472°F	61
Figure A10:	Stress-Strain curves for 100% dense I/M and 65% dense SPM of Ti-6Al-4V at 1.0 strain rate and temperature 1562°F, 1652°F, and 1742 °F	61
Figure A11:	Stress-Strain curves for 100% dense I/M and 65% dense SPM of Ti-6Al-4V at 10 strain rate and temperature 1382°F and 1472°F	63
Figure A12:	Stress-Strain curves for 100% dense I/M and 65% dense SPM of Ti-6Al-4V at 10 strain rate and temperature 1562°F, 1652°F, and 1742 °F	63

ABSTRACT

Ahmed, Shatil S. M.S. November, 1996 Department of Mechanical Engineering, Ohio University.

Study of Deformation Processing of Structural Porous Metals

The primary goal of this study is to develop a new yield function for Structural Porous Metals (SPM), which is an innovative class of material developed by McDonnell Douglas Aerospace Company. The SPM differs from conventional fully dense Ingot Metals (I/M) and partially dense Powder Metals (P/M), for the reason of having distributed closed pores and maintaining the pores after metal working which opposes the goal to densify the metal in case of P/M. Due to the structural difference the existing Yield Criteria for I/M and P/M are not applicable for SPM, and so a natural quest evolved to find a new Yield Criterion for SPM.

The yield criterion is developed by using the principle of virtual work. In this approach, all the strain energy required for deformation is accounted for. Considering the gas pressure, additional work is required to compress the gas inside the closed pores. This work term has to be added to the yield criterion. Along with yield criterion, flow rules for SPM are developed for predicting the behaviour of SPM during metal working. Experimental results on deformation processing of SPM are also discussed and compared with FEM results from a software.

Chapter 1

Introduction

Development of advanced materials for structural application in aerospace has been driven by a need to increase the strength to weight ratio. The notable recent success has been development and implementation of composite materials in structural application. But some of the recent studies indicate that composites are not the best material to be used for structural application, as they have a tendency to degrade with ageing [4, 5]. Also an increased emphasis is being placed on affordability and recyclability of these novel materials.

In the design of an ultra light weight material, the goal is to achieve increased strength to weight ratio offered by composites while maintaining the affordability of conventional metallic components. In search of such material , a partnership led by McDonnell Douglas Aerospace (MDA) is developing an innovative class of materials called Structural Porous Metals (SPM) . The basic difference between SPM and conventional composite materials lies in the fact that SPM would be developed as a

sandwich material with low density core (LDC) and two solid face sheets as a continuous cross-section within metal mill products.

Current commercial methods of producing porous metallic material result in products that are fragile due to interconnection and the angular nature of porosity. Therefore their use in structural components are restricted. At present, commercial methods can not produce large billets that can be converted to standard mill products by deformation processing. Recent development in the metal processing technology has made possible the production of SPM. This material has a potential for successfully controlling porosity characteristics in billet stock at cost comparable to standard billet production.

A process which has been successfully implemented is the low density core (LDC) process, where powder metallurgy methods are used to produce a porous sandwich core material bonded to two face-sheets. A primary feature of this process is the introduction of inert gas in the solid billet. Unlike the traditional powder metallurgy process, the trapped inert gas inside the voids is intentionally kept in LDC and it resists compressive stresses during processing. So the deformation processing of such material is not subject to the traditional yield criterion for solid ingot metals (I/M) or powder metallurgy (P/M) systems. SPM as a structural material has to go through mechanical forming processes like rolling, forging and extrusion. The deformation processing involves straining of the material beyond yield point such that plastic flow occurs. To determine the stresses required for the plastic flow, a yield criterion applicable to this material must be developed and the flow rule for this material must be known.

A fundamental need, therefore, exists for development of a new yield criterion for SPM material. The yielding of P/M material is more complicated than I/M for the reason that hydrostatic stress plays a role in yielding. For SPM it is even more complicated because in P/M the voids inside do not resist the deformation due to hydrostatic or deviatoric stress components. However the pores in SPM resist deformation, due to the fact that they are enclosed isolated pores with internal gas pressure. Thus a special yield function which takes into account the effect of hydrostatic stress and resistance of pores to deformation is required.

In this study it will be assumed that a) SPM is homogeneous and isotropic, b) no permanent change in relative density occurs up to the yield point, c) trapped gas inside pores obey the ideal gas law and show ideal fluid behaviour, d) gas pores only resist the hydrostatic stress and e) at yield point, pressure in the gas is equal to hydrostatic stress. In development of the yield criterion the principle of virtual work will be used. The starting point of this analysis is the yield criterion for conventional P/M processes [3] given by -

$$AJ_2' + BJ_1^2 = Y_R^2 \quad (1.1)$$

where J_2' is the second invariant of deviatoric stress and J_1 is the first invariant of stress tensor, Y_R is the yield stress of P/M materials, A and B are parameters which are functions of relative density R . Many researchers have determined these parameters using different semi-empirical method and experimental results. Mostly, these theories were not very successful in predicting the flow behaviour of partially dense materials [3]. Furthermore, some of these theories did not converge to the result for the simple state of

stress present under uniaxial deformation condition. A more successful approach was developed by Doraivelu et.al [3] by using the principle of virtual work. Following the same approach, the yield criterion for SPM material is developed to include the effect of enclosed pores with internal pressure.

The associated flow rule for the developed yield criterion is also derived in this study, so that the new yield criterion can be used in a finite element method to analyze the consolidation and forming of SPM.

Preparatory work is also done on incorporating the finite element method for SPM in a FEM tool called “Antares”. Finally, the experiments on rolling of SPM and compression tests were carried out in another facility (UES Inc., Dayton, Ohio). The results of the experiments are discussed and compared with FEM results. Unfortunately the experimental results are not conclusive, because of non-predictability of porosity of SPM’s produced for testing.

Chapter 2

Existing Yield Criteria

A law defining the limit of elasticity under any possible combination of stresses is known as a Yield Criterion. The concept of yield criterion is not restricted to loading directly from the annealed state, but is applicable at any state. Numerous criteria have been proposed for yielding of solids, going as far back as Coulomb in 1773, but only a few of them are acceptable and widely used. For isotropic material, those are the maximum shear theory or Tresca Criterion and the distortion energy theory or von Mises Yield Criterion. Anisotropy has been incorporated in Hill's Criterion [2].

We have assumed the SPM to be an isotropic material, so discussion of yield criterion for anisotropic material is beyond the scope of this study. Because of this isotropic behaviour, plastic yielding can then depend on magnitude of the three principal applied stresses, and not on their directions. So any yield criterion is expressible in the following form:

$$f(J_1, J_2, J_3) = K \quad (2.1a)$$

where J_1 , J_2 , and J_3 are first, second, and third invariants of the stress tensor σ_{ij} respectively and K is a known function. The invariants are commonly used in defining a state of stress. They are defined as

$$J_1 = \sigma_{11} + \sigma_{22} + \sigma_{33} \quad (2.1b)$$

$$J_2 = \sigma_{12}^2 + \sigma_{23}^2 + \sigma_{31}^2 - (\sigma_{11}\sigma_{22} + \sigma_{22}\sigma_{33} + \sigma_{33}\sigma_{11}) \quad (2.1c)$$

$$J_3 = \sigma_{11}\sigma_{22}\sigma_{33} + 2\sigma_{12}\sigma_{23}\sigma_{31} - (\sigma_{11}\sigma_{23}^2 + \sigma_{22}\sigma_{31}^2 + \sigma_{33}\sigma_{12}^2) \quad (2.1d)$$

So far the only assumption made was to treat the material as isotropic. The classical approach to finding a yield criterion for solid material is to simplify Eq. 2.1a by using the experimental result that the yielding of a solid metal is unaffected by a moderate hydrostatic stress, either applied alone or superposed on some state of combined stress [10]. This leads to the concept of deviatoric stress. It is easier in plasticity theory to break up the stress tensor into two parts, spherical stress tensor and deviatoric stress tensor. In tensor notation deviatoric stress is defined as-

$$\sigma'_{ij} = \sigma_{ij} - \sigma_m \delta_{ij} \quad (2.2)$$

where σ'_{ij} is the deviatoric stress tensor, δ_{ij} is the Kronecker's delta, σ_m is the mean stress defined as -

$$\sigma_m = \frac{1}{3} \sigma_{ii} \quad (2.3)$$

Now we can define the three invariants J'_1 , J'_2 , and J'_3 by replacing the stresses in Eq. 2.1b, 2.1c, and 2.1d respectively by deviatoric stresses as shown in Eq. 2.2. By using the concept of deviatoric stress tensor, yield criterion can be expressed in terms of second

invariant, J'_2 and third invariant, J'_3 of the deviatoric stress tensor. It should be noted that first invariant of the deviatoric stress tensor, J'_1 would be always zero, since $\sigma'_{11} + \sigma'_{22} + \sigma'_{33} = 0$ [2.2]. So Eq. 2.1 reduces to -

$$f(J'_2, J'_3) = K \quad (2.4)$$

From the above generalised form, the two most common yield criteria for solid or ingot material is briefly discussed below.

2.1 Maximum Shear Theory, or Tresca Criterion

This theory assumes that yielding will occur when the maximum shear stress reaches the value of the maximum shear stress occurring under simple tension. The Tresca criterion asserts that yielding will occur when any one of the following six conditions is reached:

$$\begin{aligned} \sigma_1 - \sigma_2 &= \pm\sigma_0 \\ \sigma_2 - \sigma_3 &= \pm\sigma_0 \\ \sigma_3 - \sigma_1 &= \pm\sigma_0 \end{aligned} \quad (2.5)$$

where σ_1, σ_2 , and σ_3 are the principal stresses and σ_0 is the principal stress in uniaxial state of stress. A plot of this yield criterion in a biaxial state is shown in Fig. 2.1.

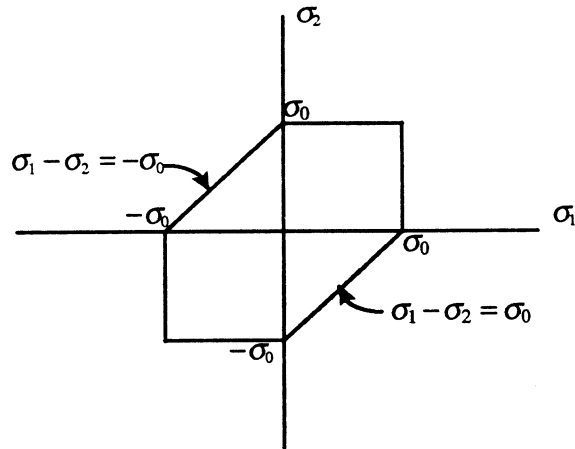


Figure 2.1

The Tresca criterion can be written in the general form of Eq. 2.4 as-

$$4J_2'^3 - 27J_3'^2 - 36k^2J_2'^2 + 96k^4J_2 - 64k^6 = 0 \quad (2.6)$$

where k is the yield in pure shear. It is to be noted that one limitation of this theory is the requirement that the yield stresses in tension and compression to be equal. For solid metals Tresca criterion is in fair agreement with experiment, but the major disadvantage is that it is necessary to know in advance which two are the maximum and minimum principal stresses.

2.2 Distortion Energy Theory, or von Mises Yield Criterion

The distortion energy theory states that yielding begins when the distortion energy equals the distortion energy in simple tension. The distortion energy U_d can be defined from

elastic strain energy, which comprises of the energy involved in changing the volume and the energy of distortion . The energy of distortion is written as-

$$U_d = \frac{1}{2G} J'_2 = \frac{1}{12G} [(\sigma_1 - \sigma_2)^2 + (\sigma_2 - \sigma_3)^2 + (\sigma_3 - \sigma_1)^2] \quad (2.7)$$

where G is the shear modulus. Now for a simple tension test $\sigma_2 = \sigma_3 = 0$ and $\sigma_1 = \sigma_0$, so U_d reduces to:

$$U_d = \frac{1}{6G} \sigma_0^2 \quad (2.8)$$

Therefore from Eq. 2.7 and 2.8, we get the famous von Mises yield criterion, given by:

$$\frac{1}{2} [(\sigma_1 - \sigma_2)^2 + (\sigma_2 - \sigma_3)^2 + (\sigma_3 - \sigma_1)^2] = \sigma_0^2 \quad (2.9)$$

A plot of the von Mises yield criterion in a biaxial state is shown in Fig. 2.2.

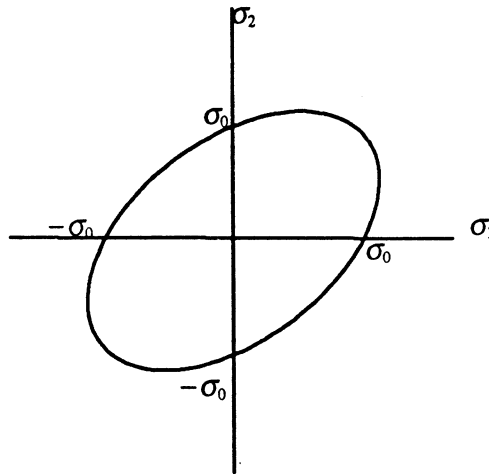


Figure2.2

The von Mises criterion can be written in the generalised form of Eq. 2.4 as

$$3J_2' = k^2 \quad (2.10)$$

Comparing Eq. 2.10 with Eq. 2.6 it is evident that von Mises criterion is far simpler and also it conforms well in experiments. But we must note that in both criteria the role of hydrostatic stress has not been taken into account, so they are applicable to fully dense or solid materials only.

2.3 Yield Criterion for Powder Metallurgy (P/M) Materials

In the case of P/M material, the onset of yielding is influenced not only by the deviatoric stress component but also the hydrostatic or spherical component. It is for this reason that the von Mises yield criterion given by Eq. 2.10 cannot be used for P/M materials. Therefore a yield function of the form

$$AJ_2' + BJ_1^2 = Y_R^2 \quad (2.11)$$

where Y_R is the yield stress of the partially dense material, has been considered by many researchers. Various researchers has derived the parameters A and B which are functions of relative density R , a table of which is available in reference [3]. However, it is observed that these functions do not always predict the observed dependence of compressive yield stress on relative density, as shown by the large discrepancies between theory and experiment. These parameters were successfully calculated by Doraivelu et.al. [3] by using the principle of virtual work. The derivation of the yield function for P/M

materials by Doraivelu et.al. is briefly repeated below, as this work on finding the yield criterion for SPM has followed the same kind of principle.

2.3.1 Derivation of Yield Function for Powder Metallurgy (P/M) Material

For partially dense P/M material, it is assumed that material is homogeneous and isotropic. Considering P/M material as continuous, it is proposed that it will yield when the apparent total deformation energy reaches a critical value. Up to the yield point, the behaviour of the P/M is considered to be linear, with no permanent change in density. For linear behaviour up to the yield point, the elastic strain energy can be written as follows:

$$w_{pm} = \frac{1}{2} \sigma_{ij} \epsilon_{ij} \quad (2.12)$$

where w_{pm} is also the work done per unit volume of P/M material, considering the body is in equilibrium so that none of this work goes into kinetic energy, then this work is stored as strain energy of deformation in the body. From elastic stress-strain relationship we can write

$$\epsilon_{ij} = \frac{(1+\nu)}{E} \sigma_{ij} - \frac{\nu}{E} \sigma_{kk} \delta_{ij} \quad (2.13)$$

where ν is the Poisson's ratio and E is the Young's modulus of the aggregate. From the definition of deviatoric stress tensor [Eq. 2.2], we can write

$$\sigma_{ij} = \sigma'_{ij} + \frac{\sigma_{kk}}{3} \delta_{ij} \quad (2.14)$$

Substituting Eq. 2.13 and 2.14 in Eq. 2.12, we get

$$w_{pm} = \frac{1}{2} \left[\left(\sigma'_{ij} + \frac{\sigma_{kk}}{3} \delta_{ij} \right) \left(\frac{1+\nu}{E} \sigma_{ij} - \frac{\nu}{E} \sigma_{kk} \delta_{ij} \right) \right] \quad (2.15)$$

after some algebraic simplification Eq. 2.15 can be written as

$$w_{pm} = \frac{1}{2} \left[\frac{1+\nu}{E} \sigma'_{ij} \sigma'_{ij} + \frac{1-2\nu}{3E} \sigma_{kk}^2 \right] \quad (2.16)$$

In Eq. 2.16 the equality of $\sigma_{ij} \sigma'_{ij} = \sigma'_{ij} \sigma'_{ij}$ has been used. Now according to this criterion, this energy is a constant at yield, independent of the stress state. Therefore like any other classical yield criterion, the strain energy can be equated to that obtained for the simple tension. For uniaxial tensile state of stress, let $\sigma_1 = Y_R$. Then the stress tensor and the deviatoric stress tensor can be represented as:

$$\sigma_{ij} = \begin{bmatrix} Y_R & 0 & 0 \\ 0 & 0 & 0 \\ 0 & 0 & 0 \end{bmatrix} \quad (2.17)$$

$$\sigma'_{ij} = \begin{bmatrix} Y_R - \frac{Y_R}{3} & 0 & 0 \\ 0 & \frac{Y_R}{3} & 0 \\ 0 & 0 & \frac{Y_R}{3} \end{bmatrix} \quad (2.18)$$

So from Eq. 2.17 and 2.18 we can easily calculate the following:

$$\sigma'_{ij} \sigma'_{ij} = \frac{2}{3} Y_R^2 \quad (2.19)$$

and

$$\sigma_{kk} = Y_R \quad (2.20)$$

Substituting the values from Eq. 2.19 and 2.20 into Eq. 2.16, we get

$$w_{pm} = \frac{1}{2} \left(\frac{3Y_R^2}{E} \right) \quad (2.21)$$

According to the criterion, equating Eq. 2.16 and 2.21 gives us

$$3(1+\nu)\sigma'_{ij}\sigma'_{ij} + (1-2\nu)\sigma_{kk}^2 = 3Y_R^2 \quad (2.22)$$

But,

$$J_2' = \frac{1}{2} \sigma'_{ij}\sigma'_{ij}$$

and,

$$J_1 = \sigma_{kk}$$

we can rewrite Eq. 2.21 as follows,

$$2(1+\nu)J_2' + \left(\frac{1-2\nu}{3} \right) J_1^2 = Y_R^2 \quad (2.23)$$

The above Eq. 2.23 represents the yield function for P/M material and it is now evident that the yield stress Y_R of the aggregate depends on the deviatoric as well as the hydrostatic stress.

Comparing Eq. 2.23 with Eq. 2.11, parameters A and B can be evaluated as,

$$A = 2(1+\nu) \quad (2.24)$$

$$B = \frac{1-2\nu}{3} \quad (2.25)$$

The next step is to relate the dependence of yield function on relative density R . A power-law dependence of Poisson's ratio ν on relative density R has been proposed by Zhadannovich [6], which states that

$$\nu = 0.5R^n \quad (2.26)$$

The value of the exponent n has been experimentally determined as approximately 2 for aluminium and ferrous powders by Kuhn [7]. For modelling purpose $n \cong 2$ is sufficiently accurate for P/M materials. Therefore, the yield function for P/M materials [Eq. 2.23] can be written in terms of relative density R as,

$$(2 + R^2)J_2' + \frac{1 - R^2}{3} J_1^2 = Y_R^2 \quad (2.27)$$

where A and B in terms of relative density R are given as,

$$A = 2 + R^2 \quad (2.28)$$

$$B = \frac{1 - R^2}{3} \quad (2.29)$$

This completes the review on existing yield criteria and the way they were derived. This is the basis for the following derivation of a new yield criterion for SPM.

Chapter 3

Yield Criterion for Structural Porous Metals (SPM)

3.1 Derivation of Yield Criterion for SPM

SPM will be treated as a homogeneous, isotropic, continuum with uniformly dispersed porosity. Additional assumptions are:

- 1) No permanent change in relative density occurs up to yield point.
- 2) Trapped gas inside pores obey ideal gas law and show ideal fluid behaviour.
- 3) Gas pores will only resist the hydrostatic stress.
- 4) At yield point pressure in gas is equal to hydrostatic stress.
- 5) Mechanical operations for SPM are isothermal.

In a P/M material the voids inside can not resist deformation due to hydrostatic or deviatoric stress components. However, the pores in SPM are closed pores with gas trapped inside, so they will resist deformation due to hydrostatic stress. In the derivation

of yield criterion for SPM , our goal is to extend it to incorporate the effect of enclosed pores with internal pressure. Using the principle of virtual work, we can express this idea as follows,

$$w_{spm} = w_{pm} + w_{gas-comp} \quad (3.1)$$

where w_{spm} is the total work done per unit volume of aggregate, w_{pm} is the work required per unit volume considering the material to be P/M, and $w_{gas-comp}$ is the additional work required to compress the gas inside the pores per unit volume of SPM. w_{pm} is already derived in the previous chapter so we will start from defining the $w_{gas-comp}$. Considering the process to be isothermal, the additional work done to compress the gas inside the pores is going to be the integral of the pressure times the small change in volume of pores:

$$\bar{w}_{gas-comp} = - \int_{\bar{v}_1}^{\bar{v}} P d\bar{v} \quad (3.2)$$

where P is the pressure inside the pores and \bar{v}_1 and \bar{v} are the initial and current volume of pores per unit mass respectively. Please note that instead of $w_{gas-comp}$, $\bar{w}_{gas-comp}$ is used to distinguish between the work done per unit volume and per unit mass respectively. This is necessary because the mass remains constant for SPM deformation, but the volume changes. The relation between the two can be given as:

$$w_{gas-comp} = \rho \bar{w}_{gas-comp} \quad (3.3)$$

where ρ is the density of the aggregate. Let R_1 and R respectively be the corresponding initial and current relative density of SPM. By definition of relative density it is the ratio between the porous material density to that of fully dense material's density, that is

$$R = \frac{\rho}{\rho_0} \quad (3.4)$$

where ρ is the density of the porous body and ρ_0 is the density of the same material if it was fully dense. Let \bar{v}_s be the volume of solid per unit total mass, then ρ_0 can be expressed as:

$$\rho_0 = \frac{1}{\bar{v}_s} \quad (3.5)$$

Let \bar{v}_p be the volume of pores per unit total mass, then ρ can be written as

$$\rho = \frac{1}{\bar{v}_s + \bar{v}_p} \quad (3.6)$$

From Eq. 3.4, 3.5, and 3.6 we can express the relative density R in terms of \bar{v}_s and \bar{v}_p as

$$R = \frac{\bar{v}_s}{\bar{v}_s + \bar{v}_p} \quad (3.7)$$

At initial state let $\bar{v}_p = \bar{v}_1$ and at current state $\bar{v}_p = \bar{v}$. Further, we will denote v_1 and v as the volume fraction of pores at initial and current state respectively. Again the relation between volume fraction of pores and volume of pores per unit mass can be written as:

$$\begin{aligned} v &= \rho \bar{v} \\ v_1 &= \rho_1 \bar{v}_1 \end{aligned} \quad (3.8)$$

where ρ_1 and ρ are the initial and current density of SPM. Considering the process to be isothermal from Gas Law, we know

$$P \bar{v} = P_1 \bar{v}_1 = \text{const.} \quad (3.9)$$

Substituting the value of P from Eq. 3.9 in Eq. 3.2, we get

$$\bar{w}_{gas_comp} = -P_1 \bar{v}_1 \int_{\bar{v}_1}^{\bar{v}} \frac{1}{\bar{v}} d\bar{v} = P_1 v_1 \ln \frac{\bar{v}_1}{\bar{v}} \quad (3.10)$$

Substituting $\frac{\bar{v}_1}{\bar{v}} = \frac{P}{P_1}$ from Eq. 3.9, Eq. 3.10 changes to

$$\bar{w}_{gas_comp} = P_1 \bar{v}_1 \ln \frac{P}{P_1} \quad (3.11)$$

Using the relation in Eq. 3.3 and Eq. 3.11, we can find w_{gas_comp} as:

$$w_{gas_comp} = \rho P_1 \bar{v}_1 \ln \frac{P}{P_1} \quad (3.12)$$

If we consider now that up to yield point the density change in SPM is very small i.e., $\rho \approx \rho_1$, then from Eq. 3.8 and Eq. 3.12 we can write

$$w_{gas_comp} = P_1 v_1 \ln \frac{P}{P_1} \quad (3.13)$$

The pressure P at yield can be assumed to be proportionate to the hydrostatic stress, so we may write

$$P = -\beta \frac{\sigma_{kk}}{3} \quad (3.14)$$

where β is an empirical parameter less than or equal to one. This may be assumed to be 1 till it can be verified by experiments, which implies that at yield the pressure inside the pores is assumed to be equal to the mean stress or hydrostatic stress. Substituting P from Eq. 3.14 in Eq. 3.13 and assuming $\beta = 1$, we get

$$w_{gas_comp} = P_1 v_1 \ln \left(-\frac{\sigma_{kk}}{3P_1} \right) \quad (3.15)$$

Now we can substitute the value of w_{pm} from Eq. 2.16 and w_{gas_comp} from Eq.3.15 in Eq. 3.1 and find the total energy required for SPM to yield:

$$w_{spm} = \frac{1}{2} \left[\frac{1+\nu}{E} \sigma'_{ij} \sigma'_{ij} + \frac{1-2\nu}{3E} \sigma_{kk}^2 \right] + P_1 \nu_1 \ln \left(-\frac{\sigma_{kk}}{3P_1} \right) \quad (3.16)$$

According to our postulated yield criterion the above energy w_{spm} should be some constant at the point of yield. Let that constant be K_1 , so we may write

$$\frac{1}{2} \left[\frac{1+\nu}{E} \sigma'_{ij} \sigma'_{ij} + \frac{1-2\nu}{3E} \sigma_{kk}^2 \right] + P_1 \nu_1 \ln \left(-\frac{\sigma_{kk}}{3P_1} \right) = K_1$$

Therefore,
$$3(1+\nu)\sigma'_{ij}\sigma'_{ij} + (1-2\nu)\sigma_{kk}^2 + 6EP_1\nu_1 \ln \left(-\frac{\sigma_{kk}}{3P_1} \right) = 6EK_1 \quad (3.17a)$$

As E can be considered to be a constant for a particular material, so we can denote the right side of Eq. 3.17a as another constant K , so Eq. 3.17a can be rewritten as

$$3(1+\nu)\sigma'_{ij}\sigma'_{ij} + (1-2\nu)\sigma_{kk}^2 + 6EP_1\nu_1 \ln \left(-\frac{\sigma_{kk}}{3P_1} \right) = K \quad (3.17b)$$

Eq. 3.17b is the Yield function for the SPM. Which reduces to the P/M yield function if there is no entrapped gas inside the pores, because in that case the third term in the above equation or w_{gas_comp} will be zero. Again if the material is considered to be 100% dense or incompressible, then $\nu = 0.5$ and the Yield function derived will reduce to von Misses yield criterion. To evaluate K , like any other yield criterion we equate Eq. 3.17b for a special case of uniaxial stress state and without pores and entrapped gas, where only stress component is Y_{spm} , in which case $\sigma'_{ij}\sigma'_{ij} = \frac{2}{3}Y_{spm}^2$ and $\sigma_{kk} = Y_{spm}$ [Eq. 2.19 and 2.20]. For uniaxial state of stress Eq. 3.17 can be written as:

$$3Y_{spm}^2 = K \quad (3.18)$$

From Eq. 3.17 and Eq. 3.18, we can write

$$3(1+\nu)\sigma'_{ij}\sigma'_{ij} + (1-2\nu)\sigma_{kk}^2 + 6EP_1\nu_1 \ln\left(-\frac{\sigma_{kk}}{3P_1}\right) = 3Y_{spm}^2 \quad (3.19)$$

we can now substitute $\sigma'_{ij}\sigma'_{ij} = 2J'_2$ and $\sigma_{kk} = J_1$ in Eq. 3.19 and get

$$6(1+\nu)J'_2 + (1-2\nu)J_1^2 + 6EP_1\nu_1 \ln\left(-\frac{J_1}{3P_1}\right) = 3Y_{spm}^2$$

$$\text{Therefore, } 2(1+\nu)J'_2 + \frac{(1-2\nu)}{3}J_1^2 + 2EP_1\nu_1 \ln\left(-\frac{J_1}{3P_1}\right) = Y_{spm}^2 = \delta Y_0^2 \quad (3.20)$$

where Y_0 is the yield stress of fully dense material and δ is a function of relative density and pressure inside the pores of the SPM material. δ has to be found experimentally.

3.2 Derivation of Flow Rule for SPM

As a first step in deriving the flow rule for SPM we need to derive the general stress-strain relations, so that none of the assumptions in deriving the flow rule contradicts the assumptions or concepts of SPM, specially the compressibility of SPM. The derivation of general stress-strain relation is intricately explained below.

3.2.1 Derivation of general stress -strain relation

We will derive the general equation for plastic stress-strain relations for any yield criterion based on a unified approach due to Drucker [8,9]. Following Drucker's approach, and using two additional assumptions, we can obtain the most general form of the plastic stress-strain relations. Let us suppose that a body is at a given state of stress and some external agency applies an additional set of stresses and which are then withdrawn slowly. Now work hardening implies that for all such added sets of stresses, the material will remain in equilibrium, and

- i. Positive work is done by the external agency during application of the set of stresses.
- ii. The net work done by the external agency over the cycle of application and withdrawal is zero or positive.

At a certain state of stress σ_{ij} and strain ϵ_{ij} , a small additional stress is applied which causes a small change in stress $d\sigma_{ij}$ and strain $d\epsilon_{ij}$ and the additional stress is withdrawn slowly. Now the strain $d\epsilon_{ij}$ consists of both elastic strain and plastic strain i.e.,

$$d\epsilon_{ij} = d\epsilon_{ij}^e + d\epsilon_{ij}^p \quad (3.21)$$

After release of load the elastic strain portion will be recovered, but the plastic strain portion will still be there and that is unrecoverable. Because of work hardening, as discussed above in (i) and (ii):

$$d\sigma_{ij}d\epsilon_{ij} > 0 \quad (3.22)$$

Therefore,
$$d\sigma_{ij}(d\varepsilon_{ij}^e + d\varepsilon_{ij}^p) > 0 \quad (3.23)$$

And

$$d\sigma_{ij}(d\varepsilon_{ij} - d\varepsilon_{ij}^e) \geq 0 \quad (3.24)$$

Therefore,
$$d\sigma_{ij}d\varepsilon_{ij}^p \geq 0 \quad (3.25)$$

Two more basic assumptions are necessary to derive the general stress-strain relations.

The assumptions are

- a) A loading function exists, which in fact is the yield function. At each state of the plastic deformation there exists a function $f(\sigma_{ij})$ so that further plastic deformation takes place only for $f(\sigma_{ij}) > K$. Both f and K may depend on the existing state of stress and strain history.
- b) The relation between infinitesimal change of stress and plastic strain is linear, i.e.,

$$d\varepsilon_{ij}^p = C_{ijkl}d\sigma_{kl} \quad (3.26)$$

The coefficient C_{ijkl} may be functions of stress, strain, and history of loading. From assumption (a) above we can write

$$\begin{aligned} df(\sigma_{ij}) &> 0 \\ \text{or } \frac{\partial f}{\partial \sigma_{ij}} d\sigma_{ij} &> 0 \end{aligned} \quad (3.27)$$

From the linearity assumption (b), we can say that if $d\sigma'_{ij}$ and $d\sigma''_{ij}$ are two increments producing plastic strain increments, $d\varepsilon_{ij}^{'p}$ and $d\varepsilon_{ij}^{'p}$, then by using the principle of

superposition, an increment $d\sigma_{ij} = d\sigma'_{ij} + d\sigma''_{ij}$ will produce an increment $(d\varepsilon'_{ij}{}^p + d\varepsilon''_{ij}{}^p)$. Now we assume that for a given state of stress σ_{kl} an incremental stress $d\sigma_{kl}$ is applied to cause plastic flow. This $d\sigma_{kl}$ can be decomposed into two components $d\sigma'_{kl}$ and $d\sigma''_{kl}$ such that the former will not cause any plastic flow and the later will be proportional to the gradient of $f(\sigma_{ij})$. Geometrically $d\sigma'_{kl}$ can be expressed as the tangent to $f(\sigma_{ij})$ and $d\sigma''_{kl}$ as the perpendicular to $f(\sigma_{ij})$.

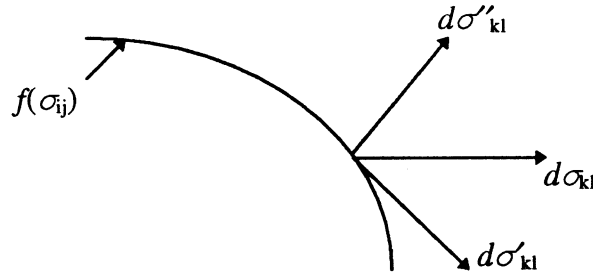


Fig. 3.1
Decomposition of incremental stress vector

As $d\sigma_{kl}$ causes a plastic flow, so from Eq. 3.27, we can write

$$\frac{\partial f}{\partial \sigma_{kl}} d\sigma_{kl} = \frac{\partial f}{\partial \sigma_{kl}} (d\sigma'_{kl} + d\sigma''_{kl}) > 0 \quad (3.28)$$

Since $d\sigma'_{kl}$ causes no plastic flow, so we can write

$$\frac{\partial f}{\partial \sigma_{kl}} d\sigma'_{kl} = 0 \quad (3.29)$$

And the $d\sigma''_{kl}$ is taken as proportional to the gradient of f . So it can be written as

$$d\sigma_{kl}'' = a \frac{\partial f}{\partial \sigma_{kl}} \quad (3.30)$$

where a is a scalar and positive. From Eq. 3.28, Eq. 3.29, and Eq. 3.30 we can write

$$\frac{\partial f}{\partial \sigma_{kl}} d\sigma_{kl} = \frac{\partial f}{\partial \sigma_{kl}} d\sigma_{kl}'' = a \frac{\partial f}{\partial \sigma_{kl}} \frac{\partial f}{\partial \sigma_{kl}} > 0 \quad (3.31)$$

now from Eq. 3.31 we can calculate a as

$$a = \frac{\frac{\partial f}{\partial \sigma_{kl}} d\sigma_{kl}}{\left(\frac{\partial f}{\partial \sigma_{mn}} \right) \left(\frac{\partial f}{\partial \sigma_{mn}} \right)} \quad (3.32)$$

If we compare Eq. 3.26 and Eq. 3.32 then we can conclude that incremental plastic strain must be proportional to a , so we may express it as

$$d\varepsilon_{ij}^p = h_{ij} a \quad (3.33)$$

where h_{ij} depends on stress, strain, and history of loading. Substituting the value of a from Eq. 3.32 in Eq. 3.33, we get

$$d\varepsilon_{ij}^p = \frac{h_{ij}}{\left(\frac{\partial f}{\partial \sigma_{mn}} \right) \left(\frac{\partial f}{\partial \sigma_{mn}} \right)} \frac{\partial f}{\partial \sigma_{kl}} d\sigma_{kl} \quad (3.34)$$

Let

$$g_{ij} = \frac{h_{ij}}{\left(\frac{\partial f}{\partial \sigma_{mn}} \right) \left(\frac{\partial f}{\partial \sigma_{mn}} \right)} \quad (3.35)$$

where g_{ij} will also be dependent on stress, strain, and history of loading. So Eq. 3.34 can be written as

$$d\epsilon_{ij}^p = g_{ij} \frac{\partial f}{\partial \sigma_{kl}} d\sigma_{kl} \quad (3.36)$$

In the same manner, in Eq. 3.25, instead of incremental plastic stress, we can use its two components and write as

$$d\sigma_{ij} d\epsilon_{ij}^p = (d\sigma'_{ij} + d\sigma''_{ij}) d\epsilon_{ij}^p \geq 0 \quad (3.37)$$

But $d\sigma'_{ij}$ produces no plastic flow. So if we multiply the component $d\sigma'_{ij}$ with a value C , where C can be positive or negative, the plastic increment $d\epsilon_{ij}^p$ will still be same. So we may write

$$(Cd\sigma'_{ij} + d\sigma''_{ij}) d\epsilon_{ij}^p \geq 0 \quad (3.38)$$

If we look at Eq. 3.38, we observe that C can be chosen a large negative number such that it will violate the condition above. Therefore, to fulfil the above condition, the term $d\sigma'_{ij} d\epsilon_{ij}^p$ must be zero. Therefore

$$d\sigma'_{ij} d\epsilon_{ij}^p = 0 \quad (3.39)$$

Substituting $d\epsilon_{ij}^p$ from Eq. 3.36 to Eq. 3.39, we get

$$d\sigma'_{ij} g_{ij} \frac{\partial f}{\partial \sigma_{kl}} d\sigma_{kl} = 0 \quad (3.40)$$

But from Eq. 3.31, we know $\frac{\partial f}{\partial \sigma_{kl}} d\sigma_{kl} > 0$. Therefore, Eq. 3.40 can be divided by

$\frac{\partial f}{\partial \sigma_{kl}} d\sigma_{kl}$ and this leads to:

$$d\sigma'_{ij} g_{ij} = 0 \quad (3.41)$$

If we compare the Eq. 3.41 to Eq. 3.29, we can write

$$g_{ij} = G \frac{\partial f}{\partial \sigma_{ij}} \quad (3.42)$$

where G is a scalar which may depend on stress, strain, and history. Substituting Eq. 3.42 in Eq. 3.46 gives

$$d\varepsilon_{ij}^p = G \frac{\partial f}{\partial \sigma_{ij}} \frac{\partial f}{\partial \sigma_{kl}} d\sigma_{kl} \quad (3.43)$$

Therefore,

$$d\varepsilon_{ij}^p = G \frac{\partial f}{\partial \sigma_{ij}} df \quad (3.44)$$

Eq. 3.44 is the general stress-strain relation.

3.2.2 Derivation of the effective plastic strain

Let stress σ_{ij} cause a strain increment of $d\varepsilon_{ij}$, then the increment in terms of the work done per unit volume can be given as

$$dw = \sigma_{ij} d\varepsilon_{ij} \quad (3.45)$$

again the strain increment can be broken into elastic and plastic components, so Eq. 3.45 can be written as

$$dw = \sigma_{ij} (d\varepsilon_{ij}^e + d\varepsilon_{ij}^p) \quad (3.46)$$

from Eq. 3.46, we can define the increment in terms of the plastic work per unit volume as:

$$dw^p = \sigma_{ij} d\varepsilon_{ij}^p \quad (3.47)$$

The definition of the effective plastic strain, we shall use is derived from the following relation between effective plastic strain increment and the plastic work per unit volume.

$$dw^p = \sigma_e d\varepsilon_p \quad (3.48)$$

from Eq. 3.47 and Eq. 3.48, we can write

$$d\varepsilon_p = \frac{1}{\sigma_e} \sigma_{ij} d\varepsilon_{ij}^p \quad (3.49)$$

We can substitute $d\varepsilon_{ij}^p$ from the general stress-strain relation in Eq. 3.44 in Eq. 3.49 and get

$$d\varepsilon_p = \frac{1}{\sigma_e} \sigma_{ij} G \frac{\partial f}{\partial \sigma_{ij}} df$$

Therefore,

$$Gdf = \frac{\sigma_e}{\sigma_{ij}} \left(\frac{\partial f}{\partial \sigma_{ij}} \right)^{-1} d\varepsilon_p = \frac{\sigma_e}{\sigma_{mn}} \left(\frac{\partial f}{\partial \sigma_{mn}} \right)^{-1} d\varepsilon_p \quad (3.50)$$

substituting Gdf in Eq. 3.44, we get

$$d\varepsilon_{ij}^p = \frac{\sigma_e}{\sigma_{mn}} \left(\frac{\partial f}{\partial \sigma_{mn}} \right)^{-1} d\varepsilon_p \frac{\partial f}{\partial \sigma_{ij}}$$

Therefore

$$d\varepsilon_{ij}^p = \frac{\sigma_e \frac{\partial f}{\partial \sigma_{ij}}}{\sigma_{mn} \left(\frac{\partial f}{\partial \sigma_{mn}} \right)} d\varepsilon_p \quad (3.51)$$

The above Eq. 3.51 gives us the relation between incremental plastic strain and incremental effective plastic strain. By differentiating Eq. 3.51 with respect to time t we

can also write the relation between plastic strain rate $\dot{\epsilon}_{ij}^p$ and the effective plastic strain rate $\dot{\epsilon}_p$ as

$$\dot{\epsilon}_{ij}^p = \frac{\sigma_e \frac{\partial f}{\partial \sigma_{ij}}}{\sigma_{mn} \left(\frac{\partial f}{\partial \sigma_{mn}} \right)} \dot{\epsilon}_p \quad (3.52)$$

3.2.3 Derivation of Stress-Strain relation for SPM

We have already defined the yield criterion for SPM in Eq. 3.20. If we denote our yield function as f , then we have

$$\left[2(1+\nu)J_2' + \frac{(1-2\nu)}{3}J_1^2 + 2EP_1\nu_1 \ln\left(-\frac{J_1}{3P_1}\right) \right]^{\frac{1}{2}} = Y_{spm} = f \quad (3.53)$$

Now to use the derived yield function in Eq. 3.52 we have to find the partial derivative of f with respect to σ_{ij} . Let us denote (similar to P/M):

$$A = 2(1+\nu) \quad (3.54)$$

$$B = \frac{(1-2\nu)}{3} \quad (3.55)$$

then using the following relations

$$\frac{\partial J_2'}{\partial \sigma_{ij}} = \sigma_{ij}', \quad \frac{\partial J_1^2}{\partial \sigma_{ij}} = 2\delta_{ij}J_1, \quad \text{and} \quad \frac{\partial J_1}{\partial \sigma_{ij}} = \delta_{ij} \quad (3.56)$$

we get

$$\frac{\partial f}{\partial \sigma_{ij}} = \frac{1}{2Y_{spm}} \left[A\sigma'_{ij} + 2B\delta_{ij}J_1 - 2EP_1\nu_1\delta_{ij} \frac{1}{J_1} \right] \quad (3.57)$$

and
$$\sigma_{mn} \frac{\partial f}{\partial \sigma_{mn}} = \frac{1}{2Y_{spm}} \left[A\sigma_{mn}\sigma'_{mn} + 2B\sigma_{mn}J_1 - 2EP_1\nu_1\sigma_{mn} \frac{1}{J_1} \right]$$

Therefore
$$\sigma_{mn} \frac{\partial f}{\partial \sigma_{mn}} = \frac{1}{2Y_{spm}} [2AJ'_2 + 2BJ_1^2 - 2EP_1\nu_1] = \frac{1}{Y_{spm}} [AJ'_2 + BJ_1^2 - EP_1\nu_1] \quad (3.58)$$

Substituting Eq. 3.57 and Eq. 3.58 in Eq. 3.52

$$\dot{\epsilon}_{ij} = \frac{\sigma_e \left(A\sigma'_{ij} + 2B\delta_{ij}J_1 - \delta_{ij} \frac{2EP_1\nu_1}{J_1} \right)}{2(AJ'_2 + BJ_1^2 - EP_1\nu_1)} \dot{\epsilon}_p \quad (3.59)$$

Let

$$E_g = \frac{EP_1\nu_1}{J_1} \quad (3.60)$$

Please note that E_g has the same unit as E , that is of stress. So we can rewrite Eq. 3.59 as

$$\dot{\epsilon}_{ij} = \frac{\sigma_e \left(A\sigma'_{ij} + 2B\delta_{ij}J_1 - 2\delta_{ij}E_g \right)}{2(AJ'_2 + BJ_1^2 - E_gJ_1)} \dot{\epsilon}_p \quad (3.61)$$

We can define the effective stress σ_e as follows:

$$\sigma_e = \frac{AJ'_2 + BJ_1^2 - E_gJ_1}{Y_{spm}} \quad (3.62)$$

Using the above definition of effective stress, Eq. 3.61 can be written as

$$\dot{\epsilon}_{ij} = \frac{\dot{\epsilon}_p}{2Y_{spm}} \left(A\sigma'_{ij} + 2B\delta_{ij}J_1 - 2\delta_{ij}E_g \right) \quad (3.63)$$

Eq. 3.63 is the associated flow rule for SPM materials.

Let

$$\frac{\dot{\epsilon}_p}{2Y_{spm}} = \dot{\lambda} \quad (3.64)$$

Substituting Eq. 3.64 in Eq. 3.63

$$\dot{\epsilon}_{ij} = \dot{\lambda} \left(A\sigma'_{ij} + 2B\delta_{ij}J_1 - 2\delta_{ij}E_g \right) \quad (3.65)$$

For simplicity of calculation if we consider the principal stresses and principal strains instead of all the components of stress and strain tensor, then Eq. 3.65 can be written for the principal directions as

$$\dot{\epsilon}_i = \dot{\lambda} \left(A\sigma'_i + 2BJ_1 - 2E_g \right) \quad (3.66)$$

Now volumetric strain rate is defined as

$$\dot{\epsilon}_v = \dot{\epsilon}_1 + \dot{\epsilon}_2 + \dot{\epsilon}_3 \quad (3.67)$$

From Eq. 3.66 we can find the values of $\dot{\epsilon}_1, \dot{\epsilon}_2,$ and $\dot{\epsilon}_3$ and find $\dot{\epsilon}_v$ from Eq. 3.67 as

$$\dot{\epsilon}_v = \dot{\lambda} \left[A(\sigma'_1 + \sigma'_2 + \sigma'_3) + 6BJ_1 - 6E_g \right]$$

Therefore,

$$\dot{\epsilon}_v = 6\dot{\lambda} \left(BJ_1 - E_g \right) \quad \left[\because \sigma'_1 + \sigma'_2 + \sigma'_3 = 0 \right] \quad (3.68)$$

From Eq. 3.68 we can write J_1 as

$$J_1 = \frac{1}{B} \left(\frac{\dot{\epsilon}_v}{6\dot{\lambda}} + E_g \right) \quad (3.69)$$

Subtracting Eq. 3.68 from Eq. 3.66, gives

$$\dot{\epsilon}_i - \dot{\epsilon}_v = \dot{\lambda} \left[A\sigma'_i - 4BJ_1 + 4E_g \right]$$

$$\text{or, } \dot{\epsilon}_i - \dot{\epsilon}_v = \dot{\lambda} \left(A\sigma_i - A\frac{J_1}{3} - 4BJ_1 + 4E_g \right)$$

Therefore,
$$3A\sigma_i = \frac{3}{\lambda}(\dot{\epsilon}_i - \dot{\epsilon}_v) + (A+12B)J_1 - 12E_s \quad (3.70)$$

Substituting J_1 from Eq. 3.69 to 3.70

$$3A\sigma_i = \frac{3}{\lambda}\dot{\epsilon}_i - \frac{3}{\lambda}\dot{\epsilon}_v + \frac{(A+12B)}{6B\lambda}\dot{\epsilon}_v - \frac{(A+12B)}{B}E_s - 12E_s$$

or,
$$\sigma_i = \frac{1}{A\lambda}\dot{\epsilon}_i + \left(\frac{A+12B}{18AB\lambda} - \frac{1}{A\lambda}\right)\dot{\epsilon}_v + \left(\frac{A+12B}{3AB} - \frac{4}{A}\right)E_s$$

Therefore,
$$\sigma_i = \frac{1}{A\lambda}\dot{\epsilon}_i + \left(\frac{A-6B}{18AB\lambda}\right)\dot{\epsilon}_v + \frac{1}{3B}E_s \quad (3.71)$$

From Eq. 3.68, we can write:

$$E_s = BJ_1 - \frac{\dot{\epsilon}_v}{6\lambda} \quad (3.72)$$

Substituting E_s from Eq. 3.72 in Eq. 3.71:

$$\sigma_i = \frac{1}{A\lambda}\dot{\epsilon}_i + \left(\frac{A-6B}{18AB\lambda}\right)\dot{\epsilon}_v - \frac{1}{18B\lambda}\dot{\epsilon}_v + \frac{J_1}{3}$$

Therefore,
$$\sigma_i = \frac{1}{A\lambda}\dot{\epsilon}_i - \frac{1}{3A\lambda}\dot{\epsilon}_v + \frac{J_1}{3} \quad (3.73)$$

If we express the strain component in terms of deviatoric strain component, then Eq. 3.73 can be expressed as:

$$\sigma_i = \frac{1}{A\lambda}\dot{\epsilon}'_i + \frac{1}{3}\left(1 - \frac{1}{A\lambda}\right)\dot{\epsilon}_v + \frac{J_1}{3} \quad (3.74)$$

And in general, the expression for the stresses induced in the SPM material can be given as:

$$\sigma_{ij} = \frac{1}{A\lambda} \dot{\epsilon}'_{ij} + \frac{1}{3} \left(1 - \frac{1}{A\lambda} \right) \delta_{ij} \dot{\epsilon}_v + \delta_{ij} \frac{J_1}{3} \quad (3.75)$$

Eq. 3.75 is the constitutive equation for SPM materials.

Chapter 4

Testing and Modification of “ANTARES” software for SPM

Our future plan involves incorporating the new yield criterion into a commercial FEM package, so that different mechanical processes like forging, rolling, extrusion, etc., can be simulated for SPM. “ANTARES” is a finite element package for solving large deformation problems encountered in manufacturing processes (developed by UES Inc., Dayton, OH). It already has features to handle forging, rolling, and extrusion for ingot material and P/M material and it is based on work flow formulation. We have chosen ANTARES as a suitable software to incorporate SPM. Preliminary investigations were carried out to resolve a number of issues.

4.1 Analysis of P/M material

To test whether ANTARES can handle P/M material correctly, a simple 2D axisymmetric model of a cylinder was created to simulate upsetting. This model is taken from a

problem solved in the book “Metal Forming and the Finite Element Method “ by S. Kobayashi et.al.[11] was chosen for verification. The results were compared to the published results [11], which were developed using another FEA application known as ALPID. Initially, a disparity was found in the two solutions. It was observed that the densification of the P/M material during upsetting was more rapid than the reference problem, although the pattern of the contours of relative density was very similar. A study of the FEA code revealed an error in the yield function for the P/M material. The error was corrected, and nearly identical simulation results, relative to those of the reference problem, were obtained. The small variation is normal, since different numerical formulations may give slightly different results. The ANTARES code now gives correct results in analysing P/M materials, and development of a numerical method for SPM products can proceed with confidence. The yield criterion for SPM materials will be an extension of the yield criterion for P/M materials. These results will be used also for making a comparison of the plastic deformation behavior of P/M and SPM materials.

4.2 Multi-Group of Elements

SPM consists of a LDC material at the center and a solid face sheet on two sides. To analyze this type of material, two kinds of material elements must be defined for the workpiece material. ANTARES has to handle two groups of elements to solve SPM forming problems. To test ANTARES’ ability to handle multiple materials, an upsetting problem with two sets of material elements was solved. It was found that the ANTARES

solver can handle multi-group of elements. The pre and post processing capabilities of the ANTARES code had to be modified slightly to store the elemental data and average the elemental results. An interface is also written to convert multi-group elements created in IDEAS (CAD software from SDRC) to a file readable to ANTARES for solving. The code is attached as Appendix B. After these modifications, the two groups of material elements worked and gave correct results.

A rolling problem was subsequently created using ANTARES. The workpiece material for simulating rolling had a dense face sheet and a LDC core material. This simulation was done to give some indication about the strain-rate range, so the strain-rate range for compression testing could be decided. The strain-rate was predicted to be in the range of 10 sec^{-1} . The relative density of the LDC material in simulation was taken as a 80% relative density P/M material, and face sheet material was 100% Ti-6Al-4V material. The P/M rolling simulation gave realistic results and provided additional confidence for proceeding in the development of the SPM yield criterion.

4.3 Multi-Stage Problem

Analysis of multi-stage problem is necessary, because most of the SPM processes will consist more than one stage. The necessary capability for multi-stage analysis is to read the rolling history from the previous stage into the next stage and repeat this process until the rolling simulation is completed. The ANTARES code was tested by simulating a rolling problem that emulated the SPM case histories that were performed in the EMPL in

May 1996 to roll the SPM cans [12]. The reduction of the billet was simulated as an eight pass process. The test case simulation again produced reasonable results.

Chapter 5

Experiments on SPM

The SPM is still in the very early stages of development, so many experiments will be necessary to determine the exact behaviour of such material in different mechanical processes. Some sub-scale processing experiments were done by UES Inc. in the Experimental Material Processing Laboratory at WPAFB using SPM billets provided by MDA [12]. This involved mainly sub-scale rolling of the SPM cans. The other major experiment performed was hot compression test of LDC of SPM. With permission from UES Inc., we have analyzed these results and did some simulations to explain the behaviours observed in the experiments.

5.1 Blister Formation in SPM can Rolling

As mentioned in the previous section the sample SPM cans produced were test rolled at EMPL in May, 1996. From the SPM rolling operations data [12], almost all the samples

rolled produced blisters that varied in size, distribution and number. Some ideas behind the blisters formation are suggested.

5.1.1 Effect of Strain-Rate

The strain-rate may effect the blistering, because, in porous and fully dense materials, strain-rate plays an important role in determining the workability of the workpiece material. It can effect the compressibility and dilatancy of porous material under compression. As a first step, the strain-rate contours in the rolling simulation were analyzed using a single group of material elements. The problem was created for two passes of rolling, and the results revealed that, in both passes, the strain-rate is of the order of 10 sec^{-1} . But, the effective strain rate contour in first pass is not same as second pass. The high-strain rate region expanded from the top surface in first pass (Fig. 5.1) towards the center of the workpiece in the second pass (Fig. 5.2). This observation may be an indication that, in the subsequent passes, the region of high strain rate increases and causes dilatation to increase the volume of LDC material. This could promote the interconnection of any isolated gas pores near the surface of the composite workpiece material. To check it further, another problem was created with two groups of material elements. Again, the face sheet material was fully dense Ti-6Al-4V and LDC material was the core material. This simulation also showed the maximum strain rate region at the interface of face sheet and LDC (Fig.5.3). This indicates that the isolated gas pores will become interconnected near the interface. It could ultimately cause the accumulated gas

to form a blister. This idea was somewhat confirmed later, when doing the compression testing of an LDC specimen at a high strain-rate of about 10 sec^{-1} , it collapsed and disintegrated.

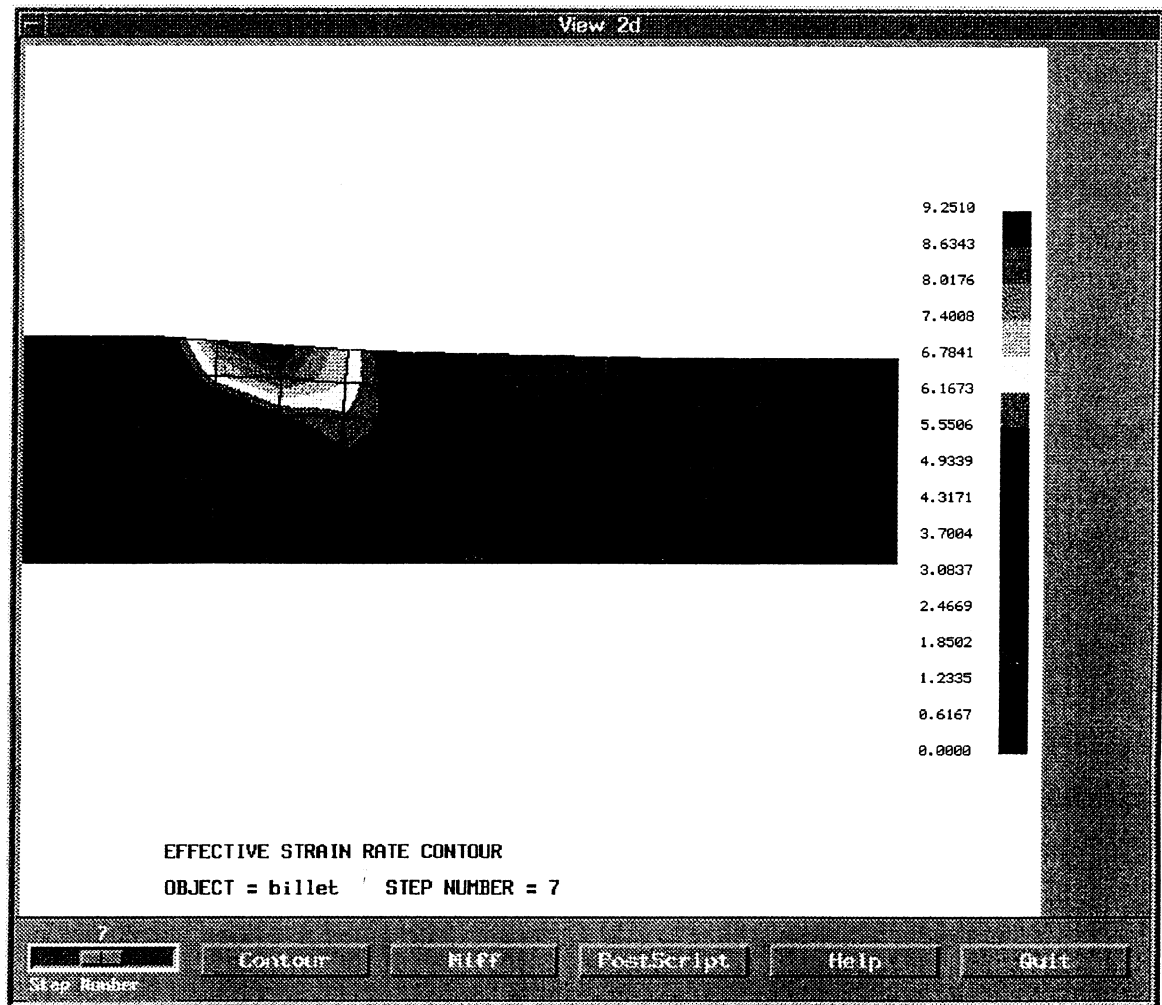


Figure 5.1

Simulated first pass of rolling showing the effective strain rate contour

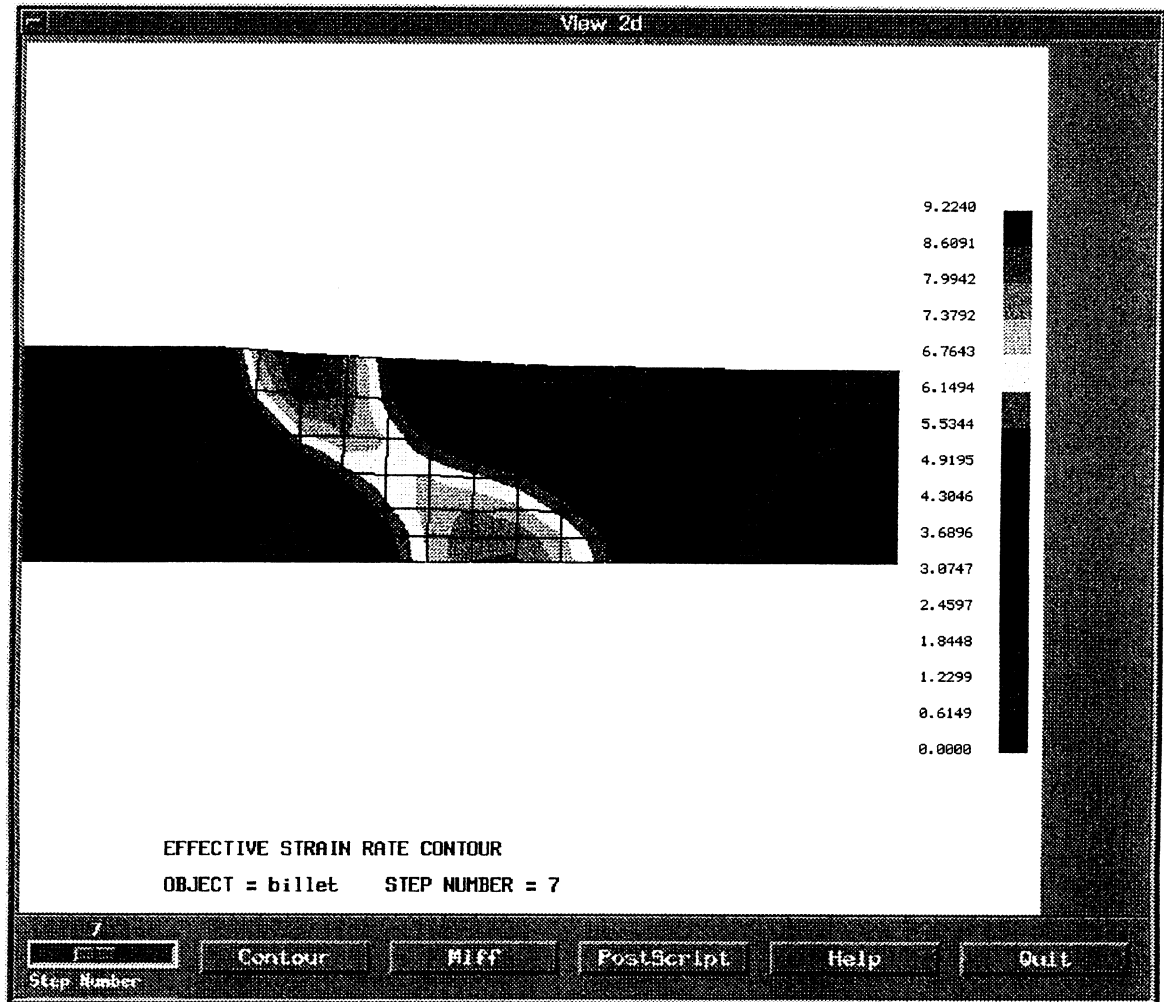


Figure 5.2

Simulated second pass of rolling showing the effective strain rate contour
expanding towards the centre of the billet

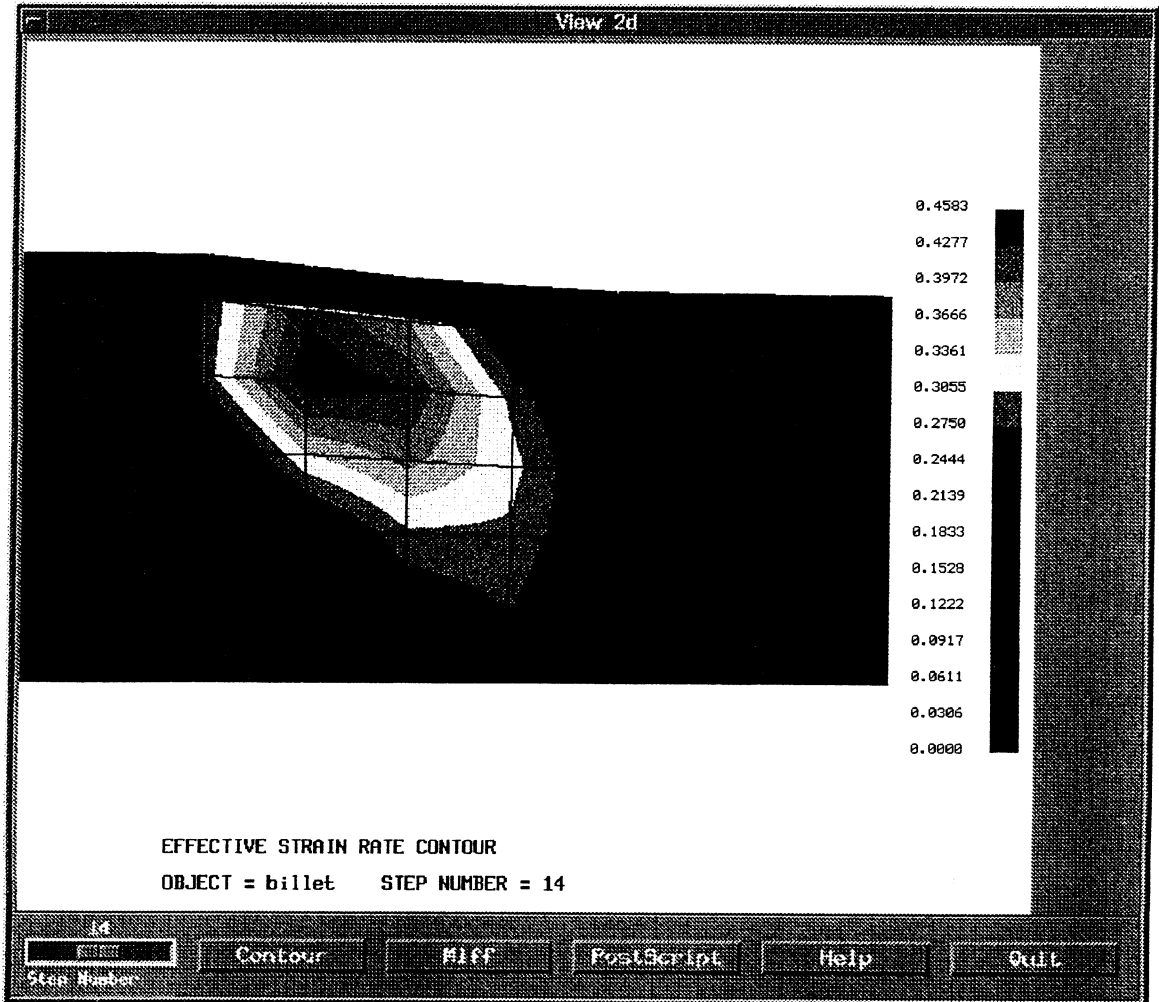


Figure 5.3

Effective strain rate contour rolling with dense face sheet

and LDC of Ti-6Al-4V

5.1.2 Effect of Differential Thermal Expansion Coefficient and Interfacial Defect

Another aspect, which was considered as a possible cause of blister formation, is the difference in thermal expansion coefficient between the face sheet and the LDC material. This difference may cause the face sheet to buckle, and this phenomenon could result in blister formation. In order for blistering to occur from buckling, a weak bond has to exist at the interface in some region. To simulate this type of situation, a model was created that had a small gap at a portion of the interface to represent the defect, and the thermal expansion coefficient was defined to be ten times more for the face sheet material than for the LDC material. The simulation did not show any sign of buckling or blistering; the defect just got pressed down further during rolling. This behavior will likely be the situation during actual rolling. Thus, a differential thermal expansion coefficient may not be an important contributing factor to the blistering process.

5.1.3 Improper sintering or bonding of the P/M material

Doubt about whether the P/M material had sintered properly in LDC material came after compression testing was performed. The compression test is described in the Appendix A. The main reasons to doubt whether proper sintering occurred during hot isostatic pressing (HIP) are as follows: (1) an unexpectedly low initial relative density was observed for a random sampling of material, and (2) a very high densification rate was observed during compression testing. If the LDC test specimens had about 20 volume

percent of isolated gas porosity, the rate of densification should be less than that for a comparable P/M material having about 20 volume percent porosity.

5.2 Compression Test of LDC of SPM

The compression tests were performed by UES personnel in the EMPL at WPAFB under the supervision of Doug Barker [13]. The samples were prepared by machining off the face sheet from both sides and EDM machining them into a cylindrical shape of size 0.378" height and 0.249" diameter. The specimens were tested at five temperatures 1382 F, 1472 F, 1562 F, 1652 F, and 1742 F, ten strain values 0.05, 0.1, 0.15, 0.2, 0.25, 0.30, 0.35, 0.4, 0.45, and 0.50, five strain-rates 0.001, 0.01, 0.1, 1.0, 10.0 sec⁻¹. The density of these materials were measured before and after compression testing. A copy of the data is attached as table 11 and 12. Though the test results were inconclusive with respect to our yield criterion, because of unexpected low initial density. The analysis done based on the compression test results is explained in Appendix 'A' for reference and continuation in future work.

Chapter 6

Conclusion and Future Work

The new yield criterion for Structural Porous Metals (SPM) was derived, which takes into account the inert gas trapped inside the isotropic homogenous pores. Using the derived yield criterion, the flow rule for SPM has been developed, which would allow incorporation of such material in existing FEM package like “ANTARES”. In this study some light has been shed on the initial experiments done on SPM, but we couldn’t verify the yield function because of the fact that the samples which were tested were unfortunately not uniform in properties. After the SPM is manufactured with the required quality, the yield criteria and flow rule will be tested experimentally. It is also encouraging that some of the suggestions made on the experiments based on the simulations are going to be followed in producing the next samples of SPM. Research must be done using LDC material that can be repeatedly reproduced.

The future work will be more towards experimenting with SPM, because to use the SPM yield criterion for the calculation of stress, an empirical relationship will have to be found between the Poisson’s ratio, the relative density, and initial pressure. To develop

this relationship, SPM samples with varying relative density will have to be fabricated. The P/M material used in those materials should be of the same consistent quality and lot. Therefore, it will be advantageous to the program if this relationship is developed using pre-alloyed Ti-6Al-4V powder to produce LDC material with different initial relative densities and pressure. Also, to validate the yield function it would be necessary to completely incorporate the flow rule in “Antares” and then simulate and compare with the sub-scale experimentation of different mechanical processes. Finally the necessary framework to represent the behaviour of SPM is now developed and in the near future the derivations here will be validated with experiments, once the appropriate kind of SPM samples are available for testing.

References

- [1] Hill, R., *Proc. Roy. Soc. London*, 193A, 1948, p. 281
- [2] Hill, R., *Mathematical Theory of Plasticity*, Chapter XII. London Oxford University Press, 1950
- [3] Doraivelu, S.M., Gegel, H.L., Gunasekera, J.S., Malas, J.C., Morgan, M.T., and Thomas J.F. Jr., "A New Yield Function for Compressible P/M Materials", *Int. J. Mech. Sci.*, Vol. 26, No. 9/10, 1984, p. 527-535.
- [4] Dao, K.C., Shockey, D.A., Seaman, L., Curran, D.R., and Rowcliffe, D.J., "Particle Impact Damage in Silicone Nitride"; Contract No. N00014-76-057, Annual Reports, Part III, Office of Naval Research, Washington, DC, May 1979
- [5] Razvan, A., and Reifsnider, K.L., "Fiber Fracture and Strength Degradation in Unidirectional Graphite/Epoxy Composite Materials", *Theoretical and Applied Fracture Mechanics*, Vol. 16, No. 1, Oct 1991, p. 81
- [6] Zhdannovich, G.M., "Theory of compacting of metal powders", Translated from *Teorizc Pressovaniya Metzllchaskikli Poroshkov*, by the Foreign Technology Division, WPAFB, Ohio, U.S.A. (Translation No. FTD-HC-23-775-70), June, 1971, p. 1-262

- [7] Kuhn, H.A., "Deformation Process of Sintered Powder Metal", Ch. 14, *Powder Metallurgy Processing: New Techniques and Analysis*, Academic Press, New York, 1978, p. 99
- [8] Drucker, D.C., "Some Implications of Work Hardening and Ideal Plasticity", *Quart. Appl. Math.*, Vol. 7, 1950, p. 411-418
- [9] Drucker, D.C., "A More Fundamental Approach to Plastic Stress-Strain Relations", *1st U.S. Congress of Applied Mechanics*, ASME, New York, 1952, p. 487-491
- [10] Polonyi, M., and Schmid, E., *Zeits, Phys.* 16, 1923, p. 336
- [11] Kobayashi, S., Oh, S.I., Altan, T., "Metal Forming and the Finite Element Method", New York, 1989, p. 249-253.
- [12] Gegel, H.L., UES Inc., Private Communication, regarding Test rolling of SPM cans in EMPL at WPAFB, on May, 1996
- [13] Gegel, H.L., UES Inc., Private Communication, regarding Compression Test of LDC of SPM performed at EMPL at WPAFB, on August, 1996

Appendix A

Results and Analysis of the Compression Test of LDC of SPM

a) Specimen Condition

Powder metal used to manufacture SPM is not prealloyed, so there is a possibility that the HIPing was not uniform and the elemental powders were not uniformly dispersed. The initial density of the specimens, which was acquired from the same batch of SPM, varied in density by $\pm 4\%$.

The initial relative density of the specimens are measured to be around 65%, an unexpected result, as the SPM samples supplied by MDA were expected to be about 80% relative density. The final relative density measured showed that all specimens were in the range of 94-99%, which is also unexpected. The SPM is supposed to maintain the initial density during mechanical operations so that it remains lighter than the conventional dense material. The size of the isolated gas porosity should be controlled by the *PV term* (Pressure times Volume), which is expected to be constant.

b) *Analysis of Experimental Data*

The stress-strain behavior of fully dense Ti-6Al-4V material was compared to the 65% dense P/M and 65% dense SPM.

The plot for Stress-Strain at strain rate 0.001sec^{-1} and different temperatures for dense, SPM, and P/M are plotted (Figure A1 & A2). In those curves, it is observed that the SPM behavior is more like the dense Ti-6Al-4V material, but the stress level is much lower. It does not exhibit any geometric hardening as does P/M materials. Another point to observe is the initial flat curve for P/M. This flatness is due to the fact that P/M has a critical relative density, which is about 0.7. The initial density of the SPM material tested was 0.65, and this value is below the critical value. Thus, the formulation actually was not valid in that region below the critical density. However, when the material is densified above the critical density, it gave correct results. A critical density will have to be established for the SPM too. This critical density will be related to the requirement for the SPM to have only isolated gas porosity and no possibility for having interconnected porosity.

Another interesting observation can be made by comparing the densification behavior of P/M material to the densification behavior of the SPM at the same strain level. At a true plastic strain level of 0.5 the relative density for P/M is 83%, whereas, after the compression test, the SPM specimens had a relative density of 94% or more. This phenomenon is not understood, but it could be related to the initial relative density or to uncontrolled metallurgical processes during HIPing.

c) Possible Errors in the Compression Test:

To confirm the initial relative density, a specimen, which was cut from the same can, was freshly measured again, using a different scale. The measured density was also in the range of 65%. Thus, there should not be any doubt about the correctness of the measured initial density of the LDC material that was tested. In addition, another specimen was cut from a different can which was kept for any repeated testing that was deemed necessary. This density was measured to be 83%, which was MDA's target initial SPM density after the HIPing process. This variance in observed initial density values after HIPing suggests that each SPM rolling can should be QA tested to assure that each can has been correctly processed.

A systematic error of about 5% was observed in the measurement of the final density after compression testing. After compression testing, the final density was somewhat larger than the initial weight measured before the test. This observation was due to the fact that glass lubricant, which was applied before testing, could not be stripped from the deformed specimen. For this reason, the error introduced was calculated not to be more than 5%, in which case, the relative density of the specimens after the test will be around 90-94%. This relative density is still higher than the maximum density that would be achieved for the case of P/M materials.

The best way to avoid the error in measuring the density after the test would be to machine the specimens to have a uniform geometry, and subsequently measure the dimensions and weight. Because the test specimens are relatively small, it may be too

difficult to machine the small specimens. The other alternative will be to measure the dimensions and weight at different strain values and before barrelling occurs.

The experimental data of hot compression test for Ti-6Al-4V of SPM is presented in tabular form in Table A2,A4,A6,A8, & A10, also the previously experimented data of fully dense Ti-6Al-4V provided by the courtesy of UES Inc. is presented in Table A1,A3,A5,A7,&A9. For comparison both sets of data has been plotted in Figure A3 through A12. These data may provide valuable information when more research is done on this growing field of SPM.

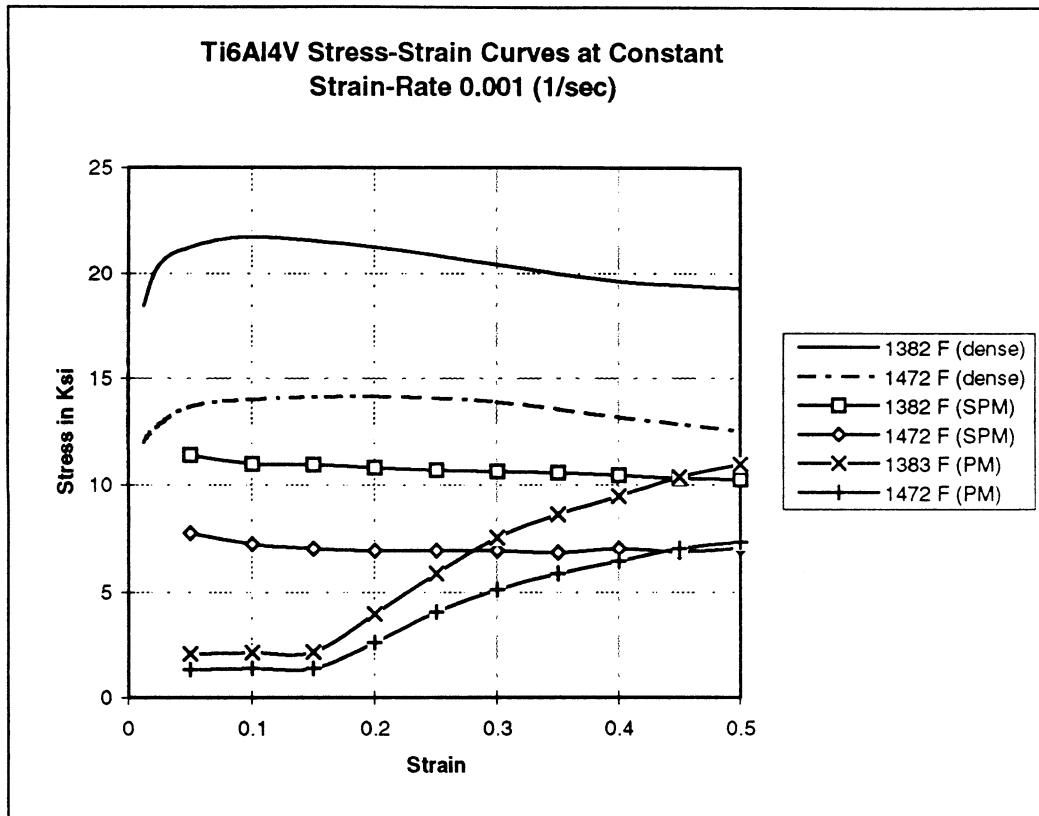


Figure A1

Comparison of Stress-Strain curves between experimental data of 100% dense Ti6Al4V, 65% dense Ti6Al4V SPM, and simulation data of 65% dense Ti6Al4V P/M at fixed strain rate 0.001 and at temperatures 1383 F and 1472 F.

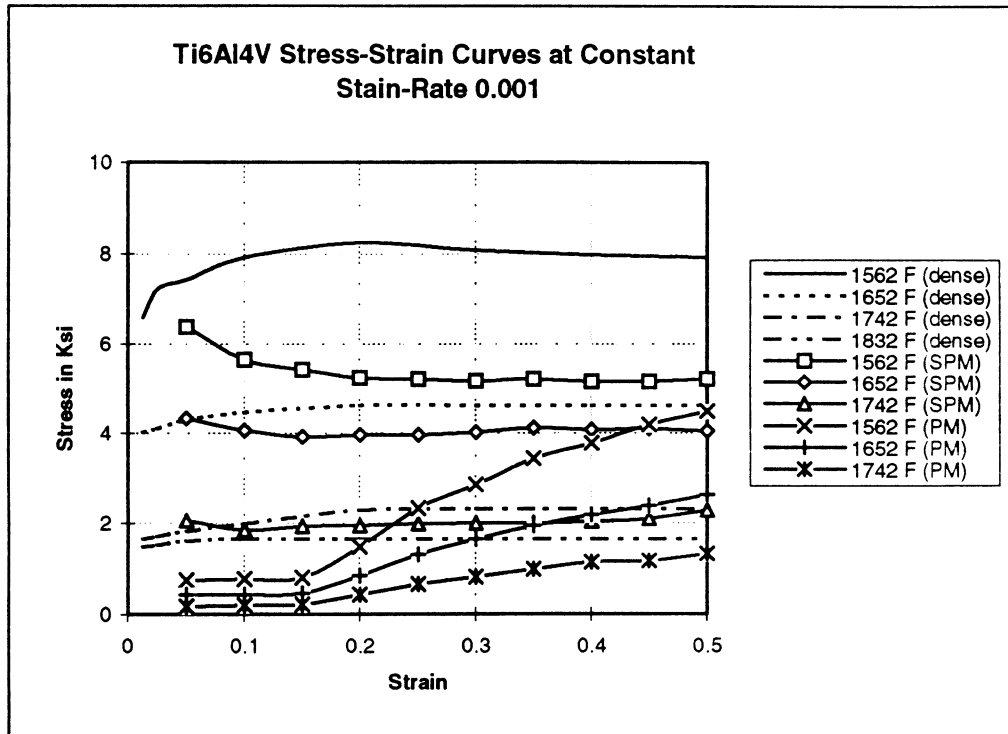


Figure A2

Comparison of Stress-Strain curves between experimental data of 100% dense Ti6Al4V, 65% dense Ti6Al4V SPM, and simulation data of 65% dense Ti6Al4V P/M at fixed strain rate 0.001 and at temperatures 1562 F, 1652 F, and 1742 F.

Table A1

Stress-Strain Table of 100% dense Ti6Al4V alloy at different temperatures and constant strain-rate 0.001 sec⁻¹

Temp. °F	Strain 0.0125	Strain 0.025	Strain 0.05	Strain 0.1	Strain 0.2	Strain 0.3	Strain 0.4	Strain 0.5
1292	18.85	20.37	20.71	20.3	19.51	18.3	17.26	16.92
1382	9.84	10.51	10.92	11.08	10.88	10.27	10.18	10.18
1472	4.66	5.18	5.7	6.34	6.56	6.56	6.47	6.39
1562	2.59	2.93	3.28	3.55	3.62	3.62	3.62	3.62
1652	1.55	1.78	1.88	2.07	2.16	2.16	2.16	2.16
1742	1.21	1.38	1.47	1.56	1.56	1.56	1.56	1.56
1832	0.77	0.91	1.04	1.21	1.14	1.04	1.04	1.04

Table A2

Stress-Strain Table of 65% SPM Ti6Al4V alloy at different temperatures and constant strain-rate 0.001 sec⁻¹

Temp. °F	Strain 0.05	Strain 0.1	Strain 0.15	Strain 0.2	Strain 0.25	Strain 0.3	Strain 0.35	Strain 0.4	Strain 0.45	Strain 0.5
1382	11.41	10.99	10.95	10.81	10.68	10.63	10.56	10.43	10.3	10.24
1472	7.73	7.21	7	6.91	6.92	6.92	6.82	7.01	6.85	7.03
1562	6.39	5.65	5.42	5.24	5.21	5.16	5.21	5.15	5.15	5.2
1652	4.33	4.05	3.92	3.96	3.96	4.02	4.12	4.07	4.1	4.04
1742	2.05	1.85	1.93	1.94	1.99	2	2	2.04	2.1	2.28

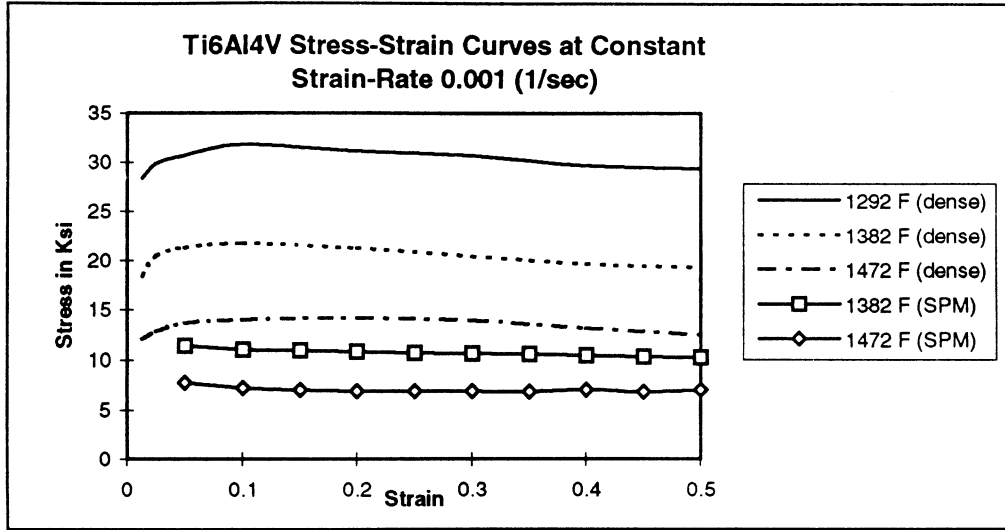


Figure A3

Comparison of Stress-Strain curves of 100% dense Ti6Al4V alloy (face-sheet of SPM) and 80% dense SPM of same alloy at 1382 °F and 1472 °F and constant strain-rate 0.001 sec⁻¹. Data for SPM at 1292 °F was not available.

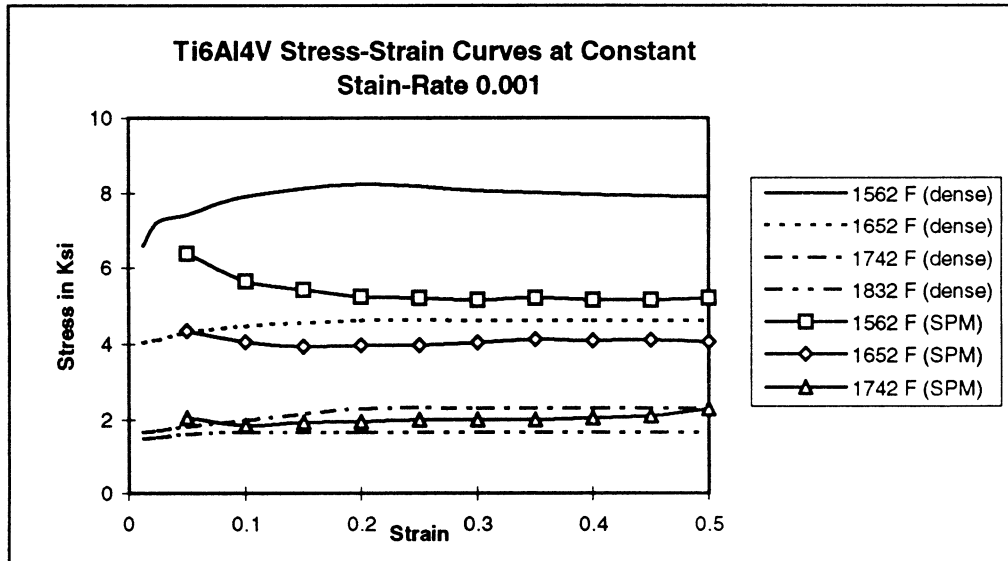


Figure A4

Comparison of Stress-Strain curves of 100% dense Ti6Al4V alloy (face-sheet of SPM) and 80% dense SPM of same alloy at 1562 °F, 1652 °F and 1742 °F and constant strain-rate 0.001 sec⁻¹. Data for SPM at 1832 °F was not available.

Table A3

Stress-Strain Table of 100% dense Ti6Al4V alloy at different temperatures and constant strain-rate 0.01 sec⁻¹

Temp. °F	Strain 0.0125	Strain 0.025	Strain 0.05	Strain 0.1	Strain 0.2	Strain 0.3	Strain 0.4	Strain 0.5
1292	38.06	39.42	40.78	42.29	43.2	43.05	42.74	42.57
1382	24.62	25.86	28.64	30.51	31.78	31.78	31.78	31.78
1472	14.45	15.1	16.61	18.12	20.69	21.3	21.75	21.75
1562	11.18	11.63	12.08	12.99	13.9	14.5	14.95	14.95
1652	7.83	7.85	7.85	7.85	7.85	7.85	7.85	7.85
1742	3.84	3.91	3.93	3.93	3.93	3.93	3.93	3.93
1832	2.87	2.94	3.02	3.02	3.02	3.02	3.02	3.02

Table A4

Stress-Strain Table of 65% SPM Ti6Al4V alloy at different temperatures and constant strain-rate 0.001 sec⁻¹

Temp. °F	Strain 0.05	Strain 0.1	Strain 0.15	Strain 0.2	Strain 0.25	Strain 0.3	Strain 0.35	Strain 0.4	Strain 0.45	Strain 0.5
1382	14.92	14.99	15.22	15.46	15.77	15.86	16.08	16.33	16.62	16.94
1472	14.53	14.01	13.78	13.68	13.65	13.69	13.72	13.75	13.82	13.81
1562	7.84	7.93	8	8.19	8.42	8.55	8.66	8.72	8.74	8.65
1652	7.16	7.03	6.96	7.05	7.04	7.11	7.21	7.24	7.31	7.26
1742	5.05	5.1	5.12	5.16	5.26	5.26	5.32	5.43	5.51	5.54

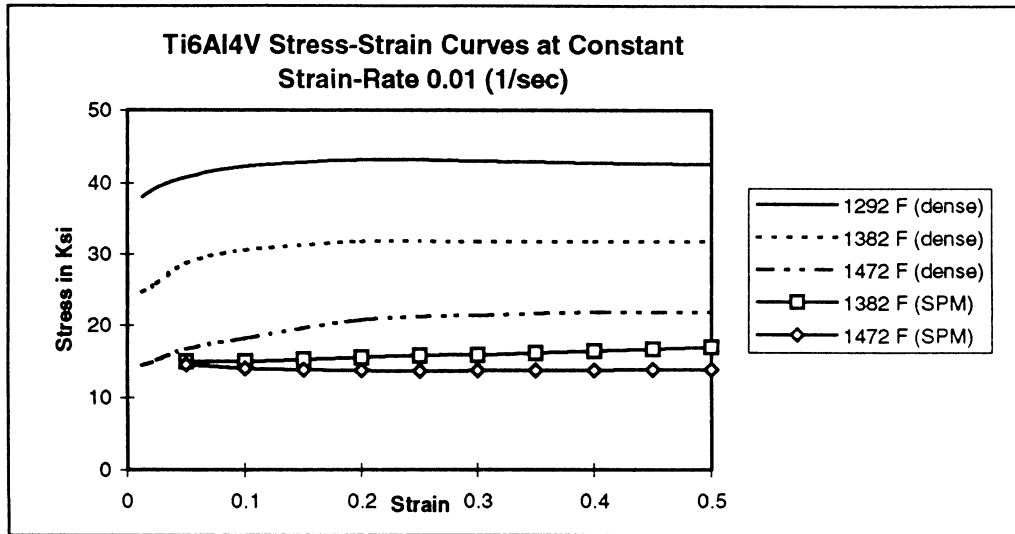


Figure A5

Comparison of Stress-Strain curves of 100% dense Ti6Al4V alloy (face-sheet of SPM) and 80% dense SPM of same alloy at 1382 °F and 1472 °F and constant strain-rate 0.01 sec⁻¹. Data for SPM at 1292 °F was not available.

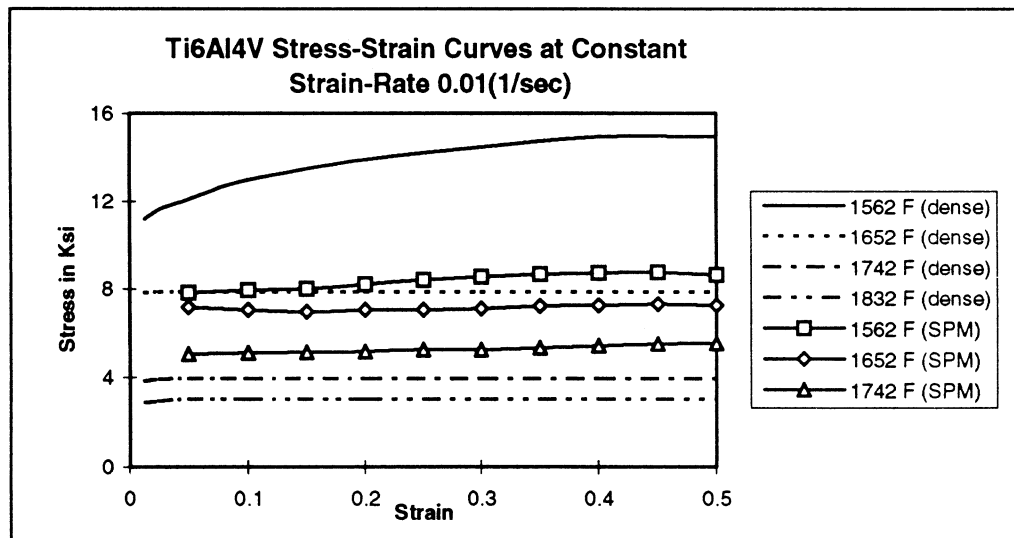


Figure A6

Comparison of Stress-Strain curves of 100% dense Ti6Al4V alloy (face-sheet of SPM) and 80% dense SPM of same alloy at 1562 °F, 1652 °F and 1742 °F and constant strain-rate 0.01 sec⁻¹. Data for SPM at 1832 °F was not available.

Table A5

Stress-Strain Table of 100% dense Ti6Al4V alloy at different temperatures and constant strain-rate 0.1 sec⁻¹

Temp. °F	Strain 0.0125	Strain 0.025	Strain 0.05	Strain 0.1	Strain 0.2	Strain 0.3	Strain 0.4	Strain 0.5
1292	45.01	46.22	47.43	48.03	47.73	47.12	46.52	46.52
1382	36.55	38.97	41.69	43.5	44.41	45.01	45.92	46.43
1472	25.83	26.68	28.13	30.21	30.96	31.72	32.78	33.35
1562	22.35	23.26	24.47	26.25	29.3	30.51	31.72	32.78
1652	9.67	9.82	9.52	9.36	9.97	10.12	10.57	10.88
1742	6.79	6.8	6.8	6.8	6.8	6.8	6.8	6.8
1832	4.53	4.64	4.89	5.44	5.87	5.95	6.04	6.04

Table A6

Stress-Strain Table of 65% SPM Ti6Al4V alloy at different temperatures and constant strain-rate 0.1 sec⁻¹

Temp. °F	Strain 0.05	Strain 0.1	Strain 0.15	Strain 0.2	Strain 0.25	Strain 0.3	Strain 0.35	Strain 0.4	Strain 0.45	Strain 0.5
1382	13.53	14.27	14.57	15.16	15.63	15.93	16.15	16.05	15.85	15.64
1472	16.41	17.28	17.57	17.61	17.68	17.84	18.1	18.28	18.69	18.88
1562	14.14	13.44	12.95	12.61	12.64	12.55	12.48	12.65	12.8	12.94
1652	12.5	11.95	11.72	11.6	11.55	11.57	11.52	11.58	11.66	11.81
1742	7.92	7.94	7.8	7.77	7.83	7.87	7.88	8.02	7.97	8.05

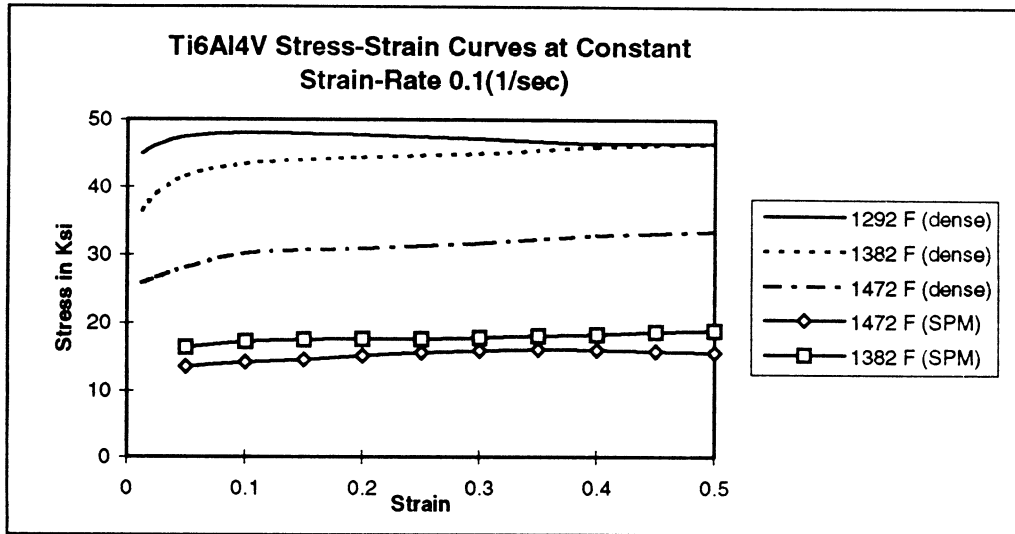


Figure A7

Comparison of Stress-Strain curves of 100% dense Ti6Al4V alloy (face-sheet of SPM) and 80% dense SPM of same alloy at 1382 °F and 1472 °F and constant strain-rate 0.1 sec⁻¹. Data for SPM at 1292 °F was not available.

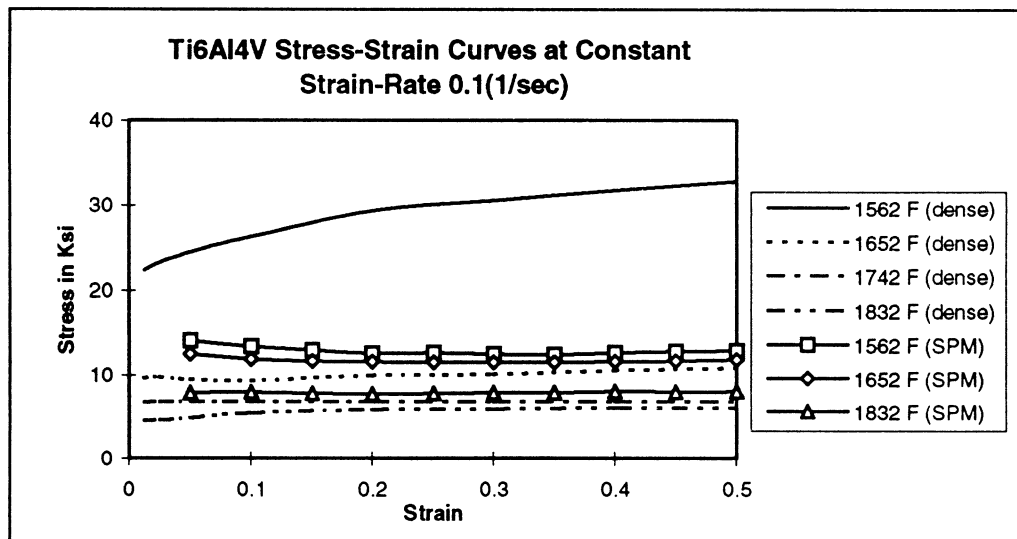


Figure A8

Comparison of Stress-Strain curves of 100% dense Ti6Al4V alloy (face-sheet of SPM) and 80% dense SPM of same alloy at 1562 °F, 1652 °F and 1742 °F and constant strain-rate 0.1 sec⁻¹. Data for SPM at 1832 °F was not available.

Table A7

Stress-Strain Table of 100% dense Ti6Al4V alloy at different temperatures and constant strain-rate 1.0 sec⁻¹

Temp. °F	Strain 0.0125	Strain 0.025	Strain 0.05	Strain 0.1	Strain 0.2	Strain 0.3	Strain 0.4	Strain 0.5
1292	52.28	54.18	56.47	58	57.31	55.14	53.23	53
1382	44.37	47.27	50.75	52.78	52.78	50.75	49.88	49.59
1472	39.15	42.34	45.02	46.54	47.27	46.4	45.53	45.24
1562	28.27	29.29	30.45	31.03	31.47	31.61	31.61	31.61
1652	19.14	20.01	20.74	21.02	21.17	21.17	21.17	21.17
1742	11.02	11.31	11.6	11.89	11.89	11.89	11.89	11.89
1832	9.21	9.79	10.15	10.51	10.73	10.73	10.73	10.73

Table A8

Stress-Strain Table of 65% SPM Ti6Al4V alloy at different temperatures and constant strain-rate 1.0 sec⁻¹

Temp. °F	Strain 0.05	Strain 0.1	Strain 0.15	Strain 0.2	Strain 0.25	Strain 0.3	Strain 0.35	Strain 0.4	Strain 0.45	Strain 0.5
1382	17.93	19.44	20.11	20.62	21.3	21.55	22	21.99	22.86	22.99
1472	16.97	18.03	18.26	18.49	19.21	18.79	19.05	18.74	19.11	19.49
1562	18.5	18.61	18.08	17.86	17.53	17.54	17.8	17.8	17.62	17.96
1652	19.12	18.77	18.91	18.46	18.38	18.47	18.25	18.4	18.15	18.45
1742	11.01	11.89	11.4	11.1	11.38	11.31	11.8	11.56	11.75	11.78

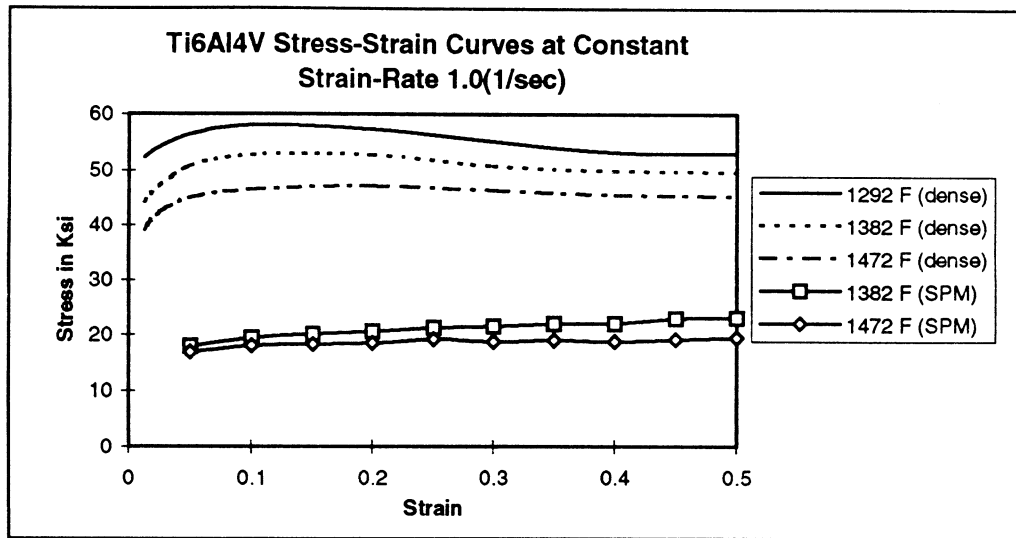


Figure A9

Comparison of Stress-Strain curves of 100% dense Ti6Al4V alloy (face-sheet of SPM) and 80% dense SPM of same alloy at 1382 °F and 1472 °F and constant strain-rate 1.0 sec⁻¹. Data for SPM at 1292 °F was not available.

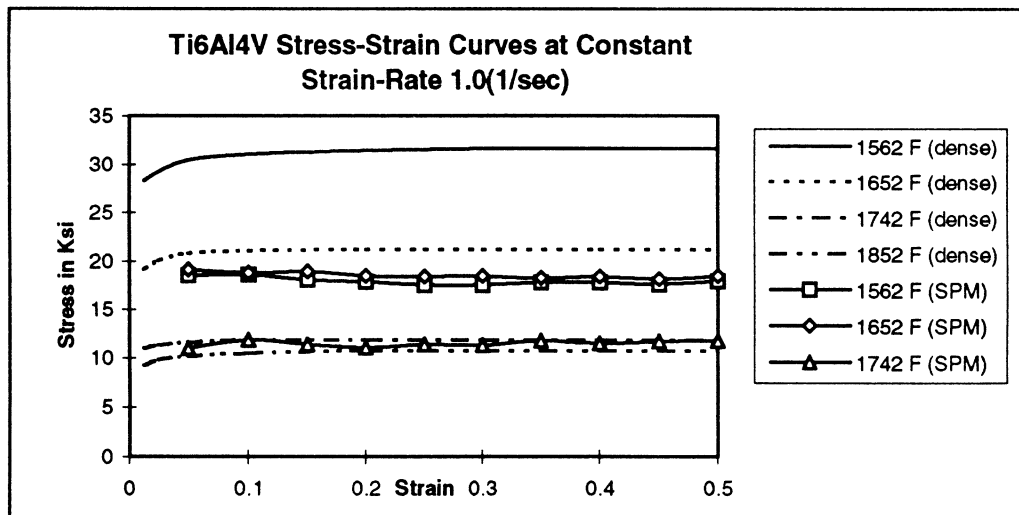


Figure A10

Comparison of Stress-Strain curves of 100% dense Ti6Al4V alloy (face-sheet of SPM) and 80% dense SPM of same alloy at 1562 °F, 1652 °F and 1742 °F and constant strain-rate 1.0 sec⁻¹. Data for SPM at 1832 °F was not available.

Table A9

Stress-Strain Table of 100% dense Ti6Al4V alloy at different temperatures and constant strain-rate 10.0 sec⁻¹

Temp F	Strain 0.0125	Strain 0.025	Strain 0.05	Strain 0.1	Strain 0.2	Strain 0.3	Strain 0.4	Strain 0.5
1292	59.71	61.41	64.4	66.96	65.81	64.82	63.54	63.54
1382	50.32	52.88	55.44	50.75	50.96	49.9	49.04	48.62
1472	43.07	44.95	46.89	50.75	50.96	49.9	49.04	48.62
1562	40.04	41.15	42.65	44.57	45.63	45.2	44.78	44.78
1652	27.35	27.68	28.36	29	29.64	29.85	30.07	30.28
1742	18.98	19.19	19.2	19.4	20.04	20.04	20.04	20.04
1832	14.5	14.2	14.5	15.35	15.95	16.21	16.63	17.06

Table A10

Stress-Strain Table of 65% SPM Ti6Al4V alloy at different temperatures and constant strain-rate 10.0 sec⁻¹

Temp F	Strain 0.05	Strain 0.1	Strain 0.15	Strain 0.2	Strain 0.25	Strain 0.3	Strain 0.35	Strain 0.4	Strain 0.45	Strain 0.5
1382	16.29	19.22	18.75	19.74	21.54	21.95	22.53	22.72	23.22	23.72
1472	23.96	26.94	25.77	26.45	27.08	27.41	27.91	27.76	28.23	28.48
1562	26.3	28.88	27.66	27.1	28.41	28.41	28.37	28.56	29.15	29.35
1652	22.14	24.66	22.42	23.7	24.12	24.04	24.72	24.69	25.37	25.53
1742	13.62	15.24	13.69	13.4	14.57	15.06	14.98	15.34	15.46	15.08

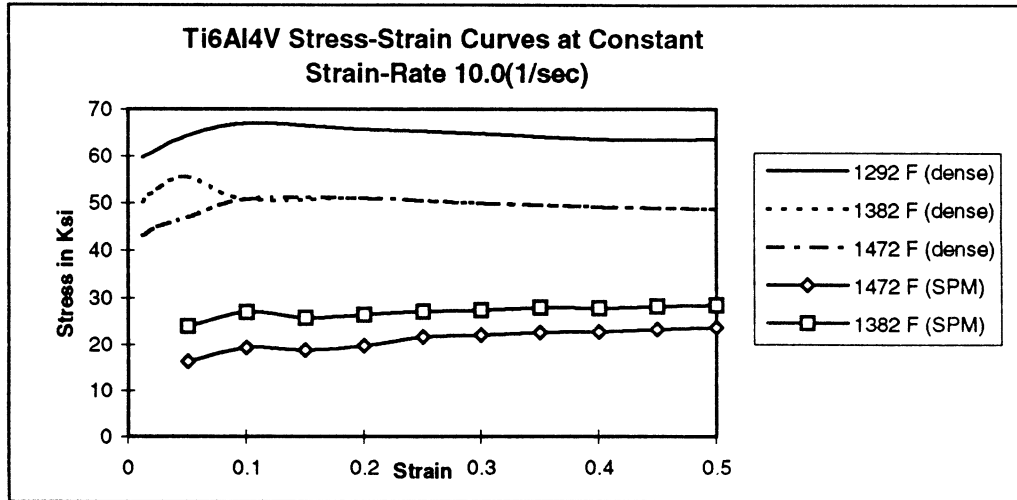


Figure A11

Comparison of Stress-Strain curves of 100% dense Ti6Al4V alloy (face-sheet of SPM) and 80% dense SPM of same alloy at 1382 °F and 1472 °F and constant strain-rate 10.0 sec⁻¹. Data for SPM at 1292 °F was not available.

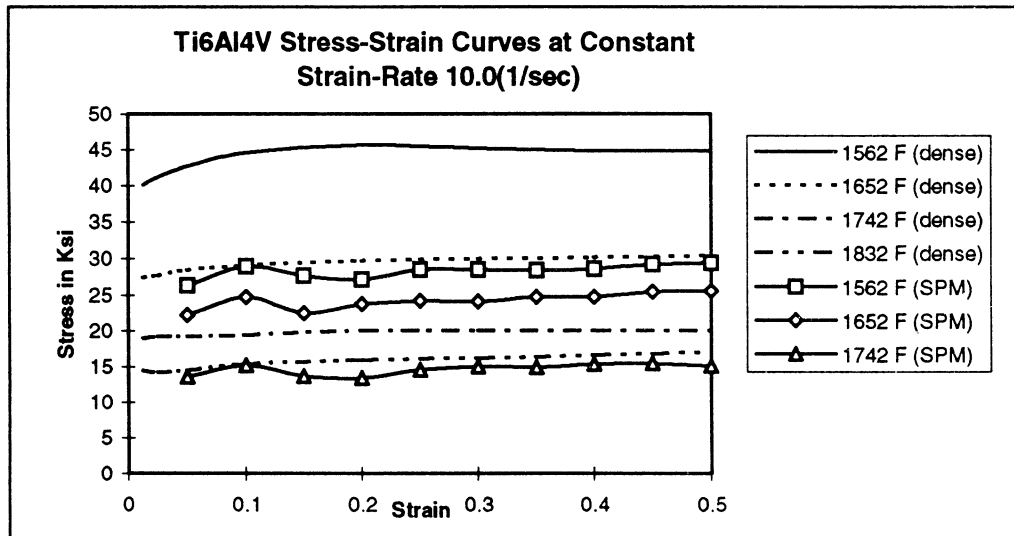


Figure A12

Comparison of Stress-Strain curves of 100% dense Ti6Al4V alloy (face-sheet of SPM) and 80% dense SPM of same alloy at 1562 °F, 1652 °F and 1742 °F and constant strain-rate 10.0 sec⁻¹. Data for SPM at 1832 °F was not available.

Table A11

Dimension and Density of LDC of SPM before the Compression test

Sample#	Weight(g)	height(cm)	Diameter(cm)	Volume(cm ³)	density(g/cm ³)
1	0.89	0.96012	0.63246	0.301756263	2.949400254
2	0.877	0.96012	0.63246	0.301756263	2.906319126
3	0.871	0.96012	0.63246	0.301756263	2.886435529
4	0.851	0.96012	0.63246	0.301756263	2.820156872
5	0.867	0.96012	0.63246	0.301756263	2.873179798
6	0.864	0.96012	0.63246	0.301756263	2.863237999
7	0.897	0.96012	0.63246	0.301756263	2.972597784
8	0.849	0.96012	0.63246	0.301756263	2.813529006
9	0.851	0.96012	0.63246	0.301756263	2.820156872
10	0.88	0.96012	0.63246	0.301756263	2.916260925
11	0.863	0.96012	0.63246	0.301756263	2.859924066
12	0.877	0.96012	0.63246	0.301756263	2.906319126
13	0.869	0.96012	0.63246	0.301756263	2.879807663
14	0.859	0.96012	0.63246	0.301756263	2.846668335
15	0.888	0.96012	0.63246	0.301756263	2.942772388
16	0.884	0.96012	0.63246	0.301756263	2.929516657
17	0.86	0.96012	0.63246	0.301756263	2.849982268
18	0.883	0.96012	0.63246	0.301756263	2.926202724
19	0.895	0.96012	0.63246	0.301756263	2.965969918
20	0.887	0.96012	0.63246	0.301756263	2.939458455
21	0.875	0.96012	0.63246	0.301756263	2.899691261
22	0.856	0.96012	0.63246	0.301756263	2.836726536
23	0.865	0.96012	0.63246	0.301756263	2.866551932
24	0.882	0.96012	0.63246	0.301756263	2.922888791
25	0.881	0.96012	0.63246	0.301756263	2.919574858
26	0.861	0.96012	0.63246	0.301756263	2.853296201
27	0.9	0.96012	0.63246	0.301756263	2.982539582
28	0.877	0.96012	0.63246	0.301756263	2.906319126
29	0.872	0.96012	0.63246	0.301756263	2.889749462
30	0.871	0.96012	0.63246	0.301756263	2.886435529
31	0.881	0.96012	0.63246	0.301756263	2.919574858
32	0.879	0.96012	0.63246	0.301756263	2.912946992
33	0.883	0.96012	0.63246	0.301756263	2.926202724
34	0.852	0.96012	0.63246	0.301756263	2.823470805

Table A11 (contd.)

Sample#	Weight(g)	height(cm)	Diameter(cm)	Volume(cm ³)	density(g/cm ³)
35	0.894	0.96012	0.63246	0.301756263	2.962655985
36	0.857	0.96012	0.63246	0.301756263	2.840040469

Table A12

Density Measurement of LDC of SPM after Compression test

Sample #	wt.in air (g)	wt.in water (g)	Post-test density (g/cm ³)	Pre-test density (g/cm ³)	%increase
1	0.9538	0.7281	4.225964	2.949401	0.432821
2	0.9173	0.6999	4.219411	2.906319	0.451806
3	0.9333	0.7227	4.431624	2.886436	0.535327
4	0.91	0.6933	4.199354	2.820157	0.48905
5	0.8863	0.6803	4.302427	2.87318	0.497444
6	0.9154	0.6848	3.969644	2.863238	0.386418
7	0.9582	0.7318	4.232332	2.972598	0.423782
8	0.89	0.67	4.045455	2.813529	0.437858
9	0.9071	0.6946	4.268706	2.820157	0.513641
10	0.8421	0.7189	6.835227	2.916261	1.343832
11	0.9163	0.6988	4.212874	2.859924	0.473072
12	0.9271	0.7165	4.402184	2.906319	0.514694
13	0.9295	0.7073	4.183168	2.879808	0.452586
14	0.898	0.6839	4.194302	2.846669	0.473407
15	0.9302	0.708	4.186319	2.942773	0.422576
16	0.9498	0.7281	4.284168	2.929517	0.462414
17	0.9328	0.721	4.404155	2.849983	0.545327
18	0.9492	0.7293	4.316508	2.926203	0.475122
19	0.9685	0.7466	4.364579	2.96597	0.471552
20	0.9629	0.74	4.319874	2.939459	0.469616
21	0.9308	0.7204	4.423954	2.899692	0.525664
22	0.9083	0.6944	4.246377	2.836727	0.496928
23	0.9229	0.7099	4.332864	2.866552	0.511524
24	0.9268	0.7068	4.212727	2.922889	0.441289
25	0.9148	0.6998	4.254884	2.919575	0.457364

APPENDIX B

Code for reading multi-group 2D elements from IDEAS to ANTARES

```

/*****
/****          group.c          ****/
/****   This is a interface to read multigroup 2D elements from IDEAS   ****/
/****   .unv format to ANTARES .geo format                               ****/
/****                                                                 ****/
/****   by: Shatil Ahmed          Date: 08/02/96          ****/
/****                                                                 ****/
/****

```

```
#include <stdio.h>
```

```
#include <stdlib.h>
```

```
#include <string.h>
```

```
#define indicator_1 " 2412\012"
```

```

#define indicator_2 "FE-BASED"
#define quad " 4"
#define surfaces 4
#define max_num_elems 1000
#define max_bound_elems 1000

main()
{
    /******* VARIABLE DECLARATIONS******/

    FILE *ifp, *ofp;
    fpos_t start_elem_line, end_elem_line, start_surf_bound, end_surf_bound, next_write;
    fpos_t title_surf_bound, title_begin, end_of_coordinate;
    char node[80], xy_coordinate[80], line[80], temp[80], elem_num[80];
    char line1[80],line2[80];
    char *pos, *pos1, *DtoE;
    int a[max_num_elems];
    int b[max_bound_elems];
    int ctr,status,i,j,f1,f2,f3,f4;
    int g1,g2,g3,g4,g5,g6;
    int node1,node2,node3,node4,max_elem_no,
        bar_elem,bar_elem_no,last_coordinate,prev_g1;
    /********/

    ifp = fopen ("ibillet.geo", "r");
    ofp = fopen ("billet.geo", "w+");

    if (ifp==NULL)

```

```

    printf("Cannot open ideas.txt for input\n");
    fprintf (ofp,"VERSION 4.1\n");
    fprintf (ofp,"Workpiece mesh file:\nRun name:\nAntares Version 4.1\n");
    fprintf (ofp,"BEGIN\n");
    fgetpos (ofp,&title_begin);
    fprintf (ofp,"
                                \n");
    fprintf (ofp,"COORDINATE DATA\n");

/*****/
/*    TRANSLATOR TO READ NODAL CO-ORDINATES FROM IDEAS    */
/*    TO ANTARES FORMAT                                    */
/*****/

    fgets (line1,79,ifp);
    while (strcspn(line1,"-")!=4)
    {
        if (strchr (line1,'.')==NULL) {
            strncpy (node,line1,10);
            strcpy (line,node);
        }
        else {
            strncpy (xy_coordinate,line1,50);
            for (i=0;i<2;i++) {
                DtoE = strchr (xy_coordinate, 'D');
                *DtoE = 'E';
            }
            strcat (line,xy_coordinate);
            fgetpos (ofp,&end_of_coordinate);
            fprintf (ofp,"%s\n",line);

```

```

    }
    fgets (line1,79,ifp);
}
fgetpos (ofp,&next_write);
fsetpos (cfp,&end_of_coordinate);
fscanf (ofp, "%d",&last_coordinate);
fsetpos (ofp,&next_write);
do {
    fgets (line1,79,ifp);
} while (strcmp (line1,indicator_1)!=0);
fprintf (ofp,"ELEMENT GROUPS  2\n");
fprintf (ofp,"ELEMENT GROUP  1      _____      __\n");

/*****
/*  TRANSLATOR TO READ FIRST GROUP OF ELEMENTS FROM          */
/*  UNIVERSAL DATASET 2411 TO ANTARES FORMAT                  */
*****/

fgetpos (ofp, &start_elem_line); /* records the starting position of element table */
fgets (line1,79,ifp);
pos1 = strstr (line1, "1      7      4");
while (pos1 == NULL)
{
    pos = strstr (line1,"2      7      4");
    if (pos != NULL) {
        strncpy (elem_num,line1,10);
        strcpy (line,elem_num);
        strcat (line, quad);
    }
}

```

```

        fscanf (ifp,"%d %d %d %d",&node4,&node3,&node2,&node1);
        fprintf (ofp,"%s %10d %10d %10d %10d\n",line,node4,node3,node2,node1);
    }
    fgets (line1,79,ifp);
    pos1 = strstr (line1, "1      7      4");
}
fprintf (ofp,"ELEMENT GROUP 2      _____      __\n");

/*****
/*  TRANSLATOR TO READ FIRST GROUP OF ELEMENTS FROM          */
/*  UNIVERSAL DATASET 2411 TO ANTARES FORMAT                  */
*****/

while (strcspn(line1,"-")!=4)
{
    if (pos1 != NULL) {
        strncpy (elem_num,line1,10);
        strcpy (line,elem_num);
        strcat (line, quad);
        fscanf (ifp,"%d %d %d %d",&node4,&node3,&node2,&node1);
        fgetpos (ofp, &end_elem_line); /* records the starting position of last line in
element table*/
        fprintf (ofp,"%s %10d %10d %10d %10d\n",line,node4,node3,node2,node1);
    }
    fgets (line1,79,ifp);
    pos1 = strstr (line1, "1      7      4");
}
fgetpos (ofp,&next_write);

```

```

fsetpos (ofp,&end_elem_line);
fscanf (ofp,"%d",&max_elem_no);
do {
    fgets (line1,79,ifp);
} while (strstr (line1,indicator_2)==NULL);
fsetpos (ofp,&next_write);
fprintf (ofp,"SURFACES  %d\n",surfaces);
fgetpos (ofp,&title_surf_bound);
fprintf (ofp,"SURFACE BOUNDARY          \n");

/*****
/*  TRANSLATOR TO READ SURFACE BOUNDARY ELEMENTS FROM      */
/*  UNIVERSAL DATASET 790 TO ANTARES FORMAT                  */
*****/

fgetpos (ofp,&next_write);
fgetpos (ofp,&start_surf_bound);
fscanf (ifp,"%d %d %d %d",&f1,&f2,&f3,&f4);
bar_elem = max_elem_no+1;
while (f1 != -1)
{
    a[f2] = bar_elem;
    fsetpos (ofp,&start_elem_line);
    prev_g1 =0;
    do {
        fscanf (ofp,"%d %d %d %d %d %d",&g1,&g2,&g3,&g4,&g5,&g6);
        if (prev_g1 == g1)
            fgets(line1,79,ofp);
        prev_g1 = g1;
    }
}

```

```
} while (g1 != f2);
switch (f3) {
    case 1:
        node1 = g3;
        node2 = g4;
        break;
    case 2:
        node1 = g4;
        node2 = g5;
        break;
    case 3:
        node1 = g5;
        node2 = g6;
        break;
    case 4:
        node1 = g6;
        node2 = g3;
        break;
    default:
        printf ("local edge of the element not within 1-4");
}
for (i=0; i<6; i++) {
    fgets (line1,79,ifp);
}
fsetpos (ofp,&next_write);
fprintf (ofp,"%6d %4d %8d %8d\n",bar_elem++, 2,node1,node2);
fgetpos (ofp,&next_write);
fscanf (ifp,"%d %d %d %d",&f1,&f2,&f3,&f4);
```

```

}
fsetpos (ofp,&title_surf_bound);
bar_elem_no = (bar_elem -1) - max_elem_no;
fprintf (ofp,"SURFACE BOUNDARY          %d",bar_elem_no);
fsetpos (ofp,&title_begin);
fprintf (ofp,"2    %d    %d    %d",last_coordinate,max_elem_no,bar_elem_no);
fsetpos (ofp,&next_write);

/*****
/*  TRANSLATOR TO READ SURFACE BOUNDARY ELEMENT NUMBERS  */
/*  FOR SURFACES ON WHICH BOUNDARY CONDITIONS ARE APPLIED  */
/*  FROM UNIVERSAL DATASET 790 TO ANTARES                      */
*****/

for (j=0; j<(surfaces-1); j++) {
    do {
        fgets (line1,79,ifp);
    } while (strstr (line1,indicator_2)==NULL);
    fscanf (ifp,"%d %d %d %d",&f1,&f2,&f3,&f4);
    ctr = 0;
    while (f1 != -1)
    {
        fsetpos (ofp,&start_elem_line);
        prev_g1 =0;
        do {
            fscanf (ofp,"%d %d %d %d %d %d",&g1,&g2,&g3,&g4,&g5,&g6);
            if (prev_g1 == g1)
                fgets(line1,79,ofp);
            prev_g1 = g1;

```

```
} while (g1 != f2);
switch (f3) {
  case 1:
    node1 = g3;
    node2 = g4;
    break;
  case 2:
    node1 = g4;
    node2 = g5;
    break;
  case 3:
    node1 = g5;
    node2 = g6;
    break;
  case 4:
    node1 = g6;
    node2 = g3;
    break;
  default:
    printf ("local edge of the element not within 1-4");
}
fsetpos (ofp, &start_surf_bound);
do {
  fscanf (ofp, "%d %d %d %d", &g1, &g2, &g3, &g4);
} while ((g3 != node1) || (g4 != node2));
b[ctr] = g1;
ctr ++ ;
for (i=0; i<6; i++) {
```

```
fgets (line1,79,ifp);
}
fscanf (ifp,"%d %d %d %d",&f1,&f2,&f3,&f4);
}
fsetpos (ofp,&next_write);
fprintf (ofp,"SURFACE S%d      %d\n",j+1,ctr);
for (i=0; i<ctr; i++) {
    fprintf (ofp,"%6d\n",b[i]);
}
fgetpos (ofp,&next_write);
}
fprintf (ofp," NODE SETS 0\n");
fprintf (ofp," ELEMENT SETS 0\n");
fprintf (ofp," ENDOBJECT");
fclose (ifp);
fclose (ofp);
}
```